Published for SISSA by Springer

Received: July 31, 2025
Accepted: September 26, 2025
Published: October 23, 2025

Modified Lüscher zeta-function and the modified effective range expansion in the presence of a long-range force

Rishabh Bubna,[a] **Hans-Werner Hammer**,[b,c] **Bai-Long Hoid**,[d] **Jin-Yi Pang**,[e,*] **Akaki Rusetsky**[a,f] **and Jia-Jun Wu**[g]

[a] *Helmholtz-Institut für Strahlen- und Kernphysik (Theorie) and Bethe Center for Theoretical Physics, Universität Bonn, 53115 Bonn, Germany*

[b] *Department of Physics, Technische Universität Darmstadt, 64289 Darmstadt, Germany*

[c] *ExtreMe Matter Institute EMMI and Helmholtz Forschungsakademie Hessen für FAIR (HFHF), GSI Helmholtzzentrum für Schwerionenforschung GmbH, 64291 Darmstadt, Germany*

[d] *Institut für Kernphysik and PRISMA$^+$ Cluster of Excellence, Johannes Gutenberg Universität, 55099 Mainz, Germany*

[e] *College of Science, University of Shanghai for Science and Technology, 200093 Shanghai, China*

[f] *Tbilisi State University, 0186 Tbilisi, Georgia*

[g] *School of Physical Sciences, University of Chinese Academy of Sciences, 100049 Beijing, China*

E-mail: bubna@hiskp.uni-bonn.de, hans-werner.hammer@physik.tu-darmstadt.de, lonbai@uni-mainz.de, jypang@usst.edu.cn, rusetsky@hiskp.uni-bonn.de, wujiajun@ucas.ac.cn

Abstract: An efficient numerical algoritm is proposed for the calculation of the modified Lüscher zeta-function in the presence of a long-range force. Using the formalism developed in ref. JHEP05(2024)168 for the analysis of synthetic data on the finite-volume energy levels in a toy model, it is demonstrated that, in contrast to the standard Lüscher approach, the truncation of the higher partial waves has very little effect on the final result. Furthermore, the regularization and renormalization of the modified Lüscher zeta-function is discussed in detail, as well as the problems arising within the cutoff regularization. It is shown that, using the renormalization scheme proposed in the present paper, one obtains modified effective range expansion parameters of natural size in all partial waves.

Keywords: Hadronic Spectroscopy, Structure and Interactions, Lattice QCD

ArXiv ePrint: 2507.18399

*Corresponding author.

https://doi.org/10.1007/JHEP10(2025)197

Contents

1 Introduction **1**

2 Modified effective range expansion and modified Lüscher equation **3**

3 Modified Lüscher zeta-function and the analysis of data **5**
3.1 Calculation of the zeta-function 5
3.2 Analysis of the synthetic data 9

4 Modified effective range expansion in the left-hand cut region **12**
4.1 Calculation of the loop function $M_\ell(q_0)$ 12
4.2 Results of numerical calculations for $M_\ell(q_0)$ 19
4.3 Coulomb interactions 21
4.4 Modified effective range expansion function 21

5 Conclusions **22**

A Partial-wave contributions to the energy shift of a given state **24**

1 Introduction

The recent surge of interest to the two-body finite-volume quantization condition in the presence of a long-range force [1–12] can be attributed, first and foremost, to the ongoing studies of two specific problems in lattice QCD. These are the calculation of the D^*D spectrum and the properties of the $T_{cc}^+(3875)$ state [13–16], as well as to the extraction of the baryon-baryon scattering phase shifts from the two-baryon spectrum [17–19].[1] At physical quark masses, both these systems feature a long-range force that emerges from the one-pion exchange. This leads to several interrelated problems in the analysis of lattice data, all stemming from the fact that the scale that defines the effective range of interactions could become sizable as compared to the inverse of the box size L. (For the systems in question, this scale is of order of the pion mass or even less.) Namely, the exponentially suppressed corrections, which are usually neglected in the derivation of the Lüscher equation [23], may become relevant. Furthermore, the standard Lüscher approach relies on the truncation of higher partial waves. However, as one knows, the convergence of the partial-wave expansion in the presence of a long-range force is poor, and many terms have to be kept in this expansion in order to achieve a reasonable accuracy. Last but not least, it is well known that the partial-wave scattering amplitudes in quantum field theory develop the so-called left-hand cut in the complex s-plane. In case of NN scattering, the beginning of this cut lies just 5 MeV below the elastic NN threshold. In general, the width of the gap between left- and right-hand cuts is related to the effective range of the interactions and is very small for the

[1] For an alternative approach to the study of these systems by using HAL QCD method, see, e.g., [20–22].

JHEP10(2025)197

systems considered here. It is also clear that, for the analysis of the energy levels which lie on or in the vicinity of the left-hand cut, the standard Lüscher method is not applicable.

In recent years, several approaches have been proposed to address the problems mentioned above. The work done within the HAL QCD approach [20–22] is conceptually very different from the rest and will not be considered here. Furthermore, a very straightforward approach, uses an effective field theory based Hamiltonian and treats long- and short-range interactions on equal footing [2]. This approach parameterizes the interactions in terms of effective couplings which are, by definition, devoid of any singularities, in contrast to the S-matrix elements. The scattering equations are then solved directly in a finite volume, producing the finite-volume spectrum that is fitted to the data. In order to avoid large partial-wave mixing effects and the emergence of the left-hand cut, the equations are solved in the plane-wave basis, without resorting to the partial-wave expansion. In this way, one also takes into account exponentially suppressed corrections, apart from those that are implicitly included in the effective couplings and are determined by a heavy scale. At the final stage, one solves the same equation in the infinite volume in order to determine S-matrix elements, using the values of the couplings extracted from the fit to the lattice spectrum. We further note that the approach, where the two-body scattering is "embedded" into the three-body problem (see, e.g., [6, 7]), is based on similar premises. Namely, below the breakup threshold, it is equivalent to the two-body equation written down in the plane-wave basis, where the sum is performed over the spectator three-momentum, while, of course, these two approaches differ above the breakup threshold. An alternative approach, using the finite-volume version of the N/D method, has also been proposed recently [8].

Another group of approaches is based on the explicit splitting of the interaction into the known long-range and the unknown short-range parts [1, 4, 5]. In particular, in this paper we shall concentrate on the approach developed in ref. [1], which uses the finite-volume generalization of the so-called modified effective range expansion by van Haeringen and Kok [24]. Here, the long-range interaction is treated in the plane-wave basis, whereas the partial-wave expansion for the short-range part is still performed. This expansion is assumed to be converging well, which will be explicitly verified below. As a result, one obtains a modified Lüscher equation with a little partial-wave mixing, which allows one to extract the scattering phase pretty much in the same way as in the standard Lüscher approach. We would like to stress that we do not plan a comparison of different approaches with the aim of determining the best one. As far as we can see, all of them are conceptually equivalent and the decision of which one to use should be based on mere convenience, see ref. [11] for more discussion on this issue.

The aim of the present paper is to demonstrate the numerical implementation of the formalism developed in ref. [1], carrying out the analysis of synthetic data generated in a toy model. In the course of this, we shall address all issues mentioned in the beginning, namely, the size of the exponentially suppressed corrections, partial-wave mixing, and the analysis of the data in the region of the left-hand cut. Another important issue that we consider in the present article is the renormalization. In particular, the modified Lüscher zeta-function, which enters the modified Lüscher equation, is given by an infinite sum of diagrams corresponding to the multiple insertions of the long-range potential into a two-particle loop. These diagrams

JHEP10(2025)197

are ultraviolet-divergent, with the degree of divergence growing with the angular momentum of a given partial wave. It can be seen that the cutoff regularization becomes inconvenient in higher partial waves, since power-law divergences force the parameters of the effective range expansion to be of an unnatural size. We therefore opt for the dimensional regularization and provide an efficient numerical algorithm for the calculation of the above-mentioned multi-loop integral in this regularization. It should be stressed that the results of these studies are relevant beyond the applications in the analysis of the finite-volume lattice data and can be used for the study of the few-body systems in the presence of several interactions with very different scales.

The layout of the paper is as follows. In order to render the paper self-contained, we review the key formulae from ref. [1] in section 2. This material is essential for the understanding of the rest of the paper. In section 3, we consider the calculation of the modified Lüscher zeta-function and the analysis of the (synthetic) data. Finally, in section 4, we consider the renormalization of the modified Lüscher zeta-function in dimensional regularization and the modified effective range expansion. To separate the conceptual issues from unnecessary technical details, we work exclusively in the center-of-mass frame and concentrate on the A_1^+ representation of the octahedral group. Furthermore, we assume that the long-range part of the potential is given by a simple Yukawa interaction corresponding to the exchange of a light particle with a mass M. Going beyond these assumptions forms the subject of a separate investigation.

2 Modified effective range expansion and modified Lüscher equation

In the infinite volume, the two-body scattering amplitude T obeys the Lippmann-Schwinger equation

$$T(\boldsymbol{p},\boldsymbol{q};q_0^2) = V(\boldsymbol{p},\boldsymbol{q}) + \int \frac{d^3\boldsymbol{k}}{(2\pi)^3}\,\frac{V(\boldsymbol{p},\boldsymbol{k})T(\boldsymbol{k},\boldsymbol{q};q_0^2)}{\boldsymbol{k}^2-q_0^2}\,, \tag{2.1}$$

where the variable q_0^2 is understood to have a small positive imaginary part, $q_0^2+i\epsilon$, above threshold as usual (q_0 denotes the magnitude of the relative three-momenta on shell). The potential $V=V_L+V_S$ is given by a sum of a long- and short-range parts. The long-range part is known and local. In the following, we assume that it is given by the Yukawa potential corresponding to the exchange of a particle with the mass M (the pion)

$$V_L(\boldsymbol{p},\boldsymbol{q}) = \frac{4\pi g}{M^2+(\boldsymbol{p}-\boldsymbol{q})^2}\,. \tag{2.2}$$

In case of the NN scattering within the chiral effective theory, for example, in the ${}^3P_0$ partial wave, $g=mM^2g_A^2/(16\pi F_\pi^2)\simeq 0.073\,m$, where m, $g_A\simeq 1.27$ and $F_\pi\simeq 92.3\,\text{MeV}$ denote the nucleon mass, axial-vector coupling constant and the pion decay constant, respectively. We shall use this value of g in the toy model considered below.

The short-range part is generally unknown and non-local. Its expansion in momenta takes the form

$$V_S(\boldsymbol{p},\boldsymbol{q}) = C_0^{00} + 3C_1^{00}\boldsymbol{p}\boldsymbol{q} + C_0^{10}(\boldsymbol{p}^2+\boldsymbol{q}^2) + \cdots\,. \tag{2.3}$$

JHEP10(2025)197

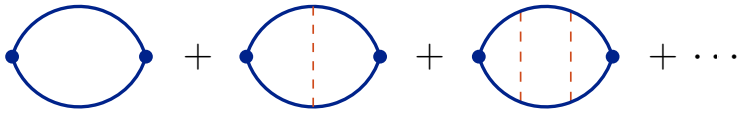

Figure 1. Perturbative expansion of the function $M_\ell(q_0)$ defined in eq. (2.5) in the coupling constant g. One-pion-exchange ladders to all orders contribute to this expansion. The filled dots correspond to the insertion of $\mathscr{Y}^*_{\ell m}(\boldsymbol{p})$ and $\mathscr{Y}_{\ell' m'}(\boldsymbol{q})$.

Note that in the derivation of the modified effective range expansion, it is usually assumed that the long-range potential is superregular. In the partial wave with angular momentum ℓ this means that $r^{-2\ell}V_L(r)$ stays analytic at $r \to 0$. The potential in eq. (2.2) does not fulfill this condition, even for $\ell = 0$. One could use different types of regularizations here, e.g., Pauli-Villars regularization as in ref. [1], or merely a sharp cutoff. As we shall see, however, this method is numerically inconvenient, when higher partial waves are included. The loops with one-pion exchanges are divergent and produce high powers of the cutoff mass. Renormalization implies that these large polynomial contributions are included in the short-range couplings $C_0^{00}, C_1^{00}, C_0^{10} \ldots$, rendering them to be unnaturally large. We shall therefore argue in favor of the dimensional regularization and introduce a renormalization scheme where such large contributions are absent from the beginning.

The modified effective range expansion for the scattering phase shift on the full potential V can be written in the following form

$$K_\ell^M(q_0^2) = M_\ell(q_0) + \frac{q_0^{2\ell+1}}{|f_\ell(q_0)|^2}\left(\cot(\delta_\ell(q_0) - \sigma_\ell(q_0)) - i\right). \tag{2.4}$$

Here, $K_\ell^M(q_0^2)$ denotes the so-called modified effective range function, whereas $M_\ell(q_0)$ is given by

$$\delta_{\ell\ell'}\delta_{mm'}M_\ell(q_0) = (4\pi)^2 \int \frac{d^3\boldsymbol{p}}{(2\pi)^3}\frac{d^3\boldsymbol{q}}{(2\pi)^3}\,\mathscr{Y}^*_{\ell m}(\boldsymbol{p})\langle \boldsymbol{p}|G_L(q_0)|\boldsymbol{q}\rangle \mathscr{Y}_{\ell' m'}(\boldsymbol{q})\,, \tag{2.5}$$

where $\mathscr{Y}_{\ell m}(\boldsymbol{p}) = p^\ell Y_{\ell m}(\hat{p})$ and $Y_{\ell m}(\hat{p})$ denotes the conventional spherical function. Furthermore, $G_L(q_0)$ is the Green function for the scattering on the long-range potential only, which obeys the following equation

$$\langle \boldsymbol{p}|G_L(q_0)|\boldsymbol{q}\rangle = \frac{(2\pi)^3\delta^3(\boldsymbol{p}-\boldsymbol{q})}{\boldsymbol{p}^2 - q_0^2} + \frac{1}{\boldsymbol{p}^2 - q_0^2}\int \frac{d^3\boldsymbol{k}}{(2\pi)^3}\,V_L(\boldsymbol{p},\boldsymbol{k})\langle \boldsymbol{k}|G_L(q_0)|\boldsymbol{q}\rangle\,. \tag{2.6}$$

Expanding the quantity $G_L(q_0)$ in perturbative series, it is seen that $M_\ell(q_0)$ is given by the sum of loops with zero, one, two,... insertions of the one-pion exchange, see figure 1. Of course, the above expressions do not make sense as they stand, since the integrals entering some of the expressions diverge in the ultraviolet. Some regularization/renormalization is implicit in these expressions. Other quantities that enter into eq. (2.4), are the phase shift on the full potential $\delta_\ell(q_0)$, the phase shift on the long-range potential $\sigma_\ell(q_0)$, and the Jost function for the long-range potential $f_\ell(q_0)$. Thus, all quantities on the right-hand side of this equation, except $\delta_\ell(q_0)$, can be evaluated from the known potential V_L prior to performing any lattice calculations. The rationale for splitting the potential into the

JHEP10(2025)197

long- and short-range parts is manifested in the properties of $K_\ell^M(q_0^2)$. Namely, while the effective range expansion of the conventional K-matrix, obtained without such a splitting, has a very small radius of convergence due to the proximity of the left-hand cut, $K_\ell^M(q_0^2)$ stays regular in the left-hand region.[2]

The modified Lüscher equation, which is based on the same splitting, performed in a finite volume, is given by $\det\left[\mathscr{A}(q_0)\right] = 0$, where

$$\mathscr{A}_{\ell m,\ell' m'}(q_0) = \frac{1}{4\pi}\,\delta_{ll'}\delta_{mm'}K_\ell^M(q_0^2) - H_{\ell m,\ell' m'}(q_0)\,. \tag{2.7}$$

In eq. (2.7), the quantity $H_{\ell m,\ell' m'}(q_0)$ is defined as (cf. with eq. (2.5))

$$H_{\ell m,\ell' m'}(q_0) = \frac{4\pi}{L^6}\sum_{\boldsymbol{p},\boldsymbol{q}} \mathscr{Y}^*_{\ell m}(\boldsymbol{p})\langle \boldsymbol{p}|G_L(q_0)|\boldsymbol{q}\rangle \mathscr{Y}_{\ell' m'}(\boldsymbol{q})\,, \tag{2.8}$$

where $G_L(q_0)$ is given by eq. (2.6), with the integration replaced by summation over the discrete momenta $\boldsymbol{p} = 2\pi\boldsymbol{n}/L\,,\ \boldsymbol{q} = 2\pi\boldsymbol{n'}/L\,,$ with $\boldsymbol{n}\,,\boldsymbol{n'} \in \mathbb{Z}^3$.

Owing to the lack of the rotational invariance, the finite-volume quantization condition is not diagonal in angular momentum. Partial diagonalization is achieved using the octahedral symmetry of the cubic lattice. To this end, one defines (see, e.g., [23, 25, 26])

$$\delta_{\sigma\rho}\mathscr{A}^\Gamma_{t\ell,t'\ell'}(q_0) = \sum_{mm'}\left(c^{\Gamma\sigma t}_{\ell m}\right)^* \mathscr{A}_{\ell m,\ell' m'}(q_0)c^{\Gamma\rho t'}_{\ell' m'}\,. \tag{2.9}$$

Here, Γ denotes a particular irreducible representation (irrep) of the octahedral group, and t, t' are indices that label different copies of the same irrep Γ contained in the irreps of the rotation group characterized by angular momenta ℓ, ℓ' respectively. Furthermore, σ, ρ label basis vectors in the irrep Γ, and $c^{\Gamma\sigma t}_{\ell m}$, $c^{\Gamma\rho t'}_{\ell' m'}$ denote the pertinent Clebsh-Gordan coefficients. The quantization condition in a given irrep is now given by $\det\left[\mathscr{A}^\Gamma(q_0)\right] = 0$. Finally, the spherical harmonics after the projection onto the irrep Γ are defined as

$$\mathscr{Y}^{\Gamma\sigma t}_\ell(\boldsymbol{p}) = \sum_m c^{\Gamma\sigma t}_{\ell m}\mathscr{Y}_{\ell m}(\boldsymbol{p})\,. \tag{2.10}$$

Owing to the Wigner-Eckart theorem, the sum in the r.h.s. of eq. (2.9) yields the factor $\delta_{\sigma\rho}$ with the coefficient that does not depend on σ and ρ. For this reason, one may fix $\sigma = \rho$ to any value in the calculations. For this reason, and in order to avoid clutter of indices, in the following we suppress σ, ρ in all expressions.

3 Modified Lüscher zeta-function and the analysis of data

3.1 Calculation of the zeta-function

In this section we shall concentrate on the calculation of the quantity that enters the matrix $\mathscr{A}^\Gamma_{t\ell,t'\ell'}(q_0)$ from eq. (2.9):

$$H^\Gamma_{t\ell,t'\ell'}(q_0) = \frac{4\pi}{L^6}\sum_{\boldsymbol{p},\boldsymbol{q}}\left(\mathscr{Y}^{\Gamma t}_\ell(\boldsymbol{p})\right)^*\langle \boldsymbol{p}|G_L(q_0)|\boldsymbol{q}\rangle \mathscr{Y}^{\Gamma t'}_{\ell'}(\boldsymbol{q})\,. \tag{3.1}$$

[2] Note also that the conventional effective-range expansion is obtained from eq. (2.4) by assuming $M_\ell(q_0) = iq_0^{2\ell+1}$, $f_\ell(q_0) = 1$ and $\sigma_\ell(q_0) = 0$. The conventional K-matrix is defined as $K_\ell(q_0^2) = q_0^{2\ell+1}\cot\delta_\ell(q_0)$, where the phase shift $\delta_\ell(q_0)$ is the same as in eq. (2.4).

JHEP10(2025)197

In the infinite volume, the summation is replaced by integration, and we have

$$\begin{aligned} H^{\Gamma,\infty}_{t\ell,t'\ell'}(q_0) &= \sum_{mm'} \left(c^{\Gamma t}_{\ell m}\right)^* H^{\infty}_{\ell m,\ell' m'}(q_0) c^{\Gamma t'}_{\ell' m'} \\ &= \frac{1}{4\pi} \sum_{mm'} \left(c^{\Gamma t}_{\ell m}\right)^* \delta_{\ell\ell'}\delta_{mm'} \mathrm{Re}\left[M_\ell(q_0)\right] c^{\Gamma t'}_{\ell' m'} \\ &= \frac{1}{4\pi}\, \delta_{\ell\ell'}\delta_{mm'}\delta_{tt'} \mathrm{Re}\left[M_\ell(q_0)\right] \,. \end{aligned} \tag{3.2}$$

One further defines

$$\begin{aligned} \Delta H^{\Gamma}_{t\ell,t'\ell'}(q_0) &= H^{\Gamma}_{t\ell,t'\ell'}(q_0) - H^{\Gamma,\infty}_{t\ell,t'\ell'}(q_0) \\ &= H^{\Gamma}_{t\ell,t'\ell'}(q_0) - \frac{1}{4\pi}\, \delta_{\ell\ell'}\delta_{tt'} \mathrm{Re}\left[M_\ell(q_0)\right] \,. \end{aligned} \tag{3.3}$$

The matrix that enters in the quantization condition, takes the form

$$\mathscr{A}^{\Gamma}_{t\ell,t'\ell'}(q_0) = \frac{1}{4\pi}\, \delta_{\ell\ell'}\delta_{tt'} K^M_\ell(q_0^2) - H^{\Gamma}_{t\ell,t'\ell'}(q_0) \,. \tag{3.4}$$

Using eq. (2.4) and the unitarity relation, which relates the imaginary part of $M_\ell(q_0)$ with the Jost function $f_\ell(q_0)$, the matrix $\mathscr{A}$ can be finally rewritten in the following form

$$\mathscr{A}^{\Gamma}_{t\ell,t'\ell'}(q_0) = \frac{q_0^{2\ell+1}}{4\pi |f_\ell(q_0)|^2}\, \delta_{\ell\ell'}\delta_{tt'} \cot(\delta_\ell(q_0) - \sigma_\ell(q_0)) - \Delta H^{\Gamma}_{t\ell,t'\ell'}(q_0) \,. \tag{3.5}$$

The advantage of this transformation consists in the fact that the quantity ΔH does not contain ultraviolet divergences. Indeed, let us consider the quantity $G_L(q_0)$, which enters the expression of the matrix H. The free Green function in the finite-volume version of the Lippmann-Schwinger equation (2.6) can be split into two parts, according to

$$\frac{1}{\boldsymbol{p}^2 - q_0^2} = \underbrace{\left(\frac{1}{\boldsymbol{p}^2 + \mu^2} + \frac{\mu^2 + q_0^2}{(\boldsymbol{p}^2 + \mu^2)^2} + \cdots + \frac{(\mu^2 + q_0^2)^n}{(\boldsymbol{p}^2 + \mu^2)^{n+1}} \right)}_{=G_1} + \underbrace{\frac{(\mu^2 + q_0^2)^{n+1}}{(\boldsymbol{p}^2 + \mu^2)^{n+1}(\boldsymbol{p}^2 - q_0^2)}}_{=G_2} \,. \tag{3.6}$$

Here, μ is an arbitrary scale, and the number of the subthreshold subtractions n is taken large enough to ensure the ultraviolet convergence of all sums after the angular-momentum truncation, when G_L is replaced by G_2. Furthermore, defining the scattering amplitude T_1 through the Lippmann-Schwinger equation $T_1 = V_L + V_L G_1 T_1$, we get

$$G_L = \underbrace{G_1 + G_1 T_1 G_1}_{=G_\mu} + \underbrace{(1 + G_1 T_1)\tilde{G}(T_1 G_1 + 1)}_{=G_f} \,, \tag{3.7}$$

where

$$\tilde{G} = G_2 + G_2 T_1 \tilde{G} \,. \tag{3.8}$$

The infinite-volume limit in the above equations are easily performed by replacing sums by integrals. Then, we have

$$\begin{aligned} \Delta H^{\Gamma}_{t\ell,t'\ell'}(q_0) = \frac{4\pi}{L^6} \sum_{\boldsymbol{p},\boldsymbol{q}} \left(\mathscr{Y}^{\Gamma t}_\ell(\boldsymbol{p})\right)^* \langle \boldsymbol{p}| G_\mu(q_0) + G_f(q_0) |\boldsymbol{q}\rangle \mathscr{Y}^{\Gamma t'}_{\ell'}(\boldsymbol{q}) \\ -4\pi \int \frac{d^3\boldsymbol{p}}{(2\pi)^3} \frac{d^3\boldsymbol{q}}{(2\pi)^3} \left(\mathscr{Y}^{\Gamma t}_\ell(\boldsymbol{p})\right)^* \langle \boldsymbol{p}| G^\infty_\mu(q_0) + G^\infty_f(q_0) |\boldsymbol{q}\rangle \mathscr{Y}^{\Gamma t'}_{\ell'}(\boldsymbol{q}) \,. \end{aligned} \tag{3.9}$$

JHEP10(2025)197

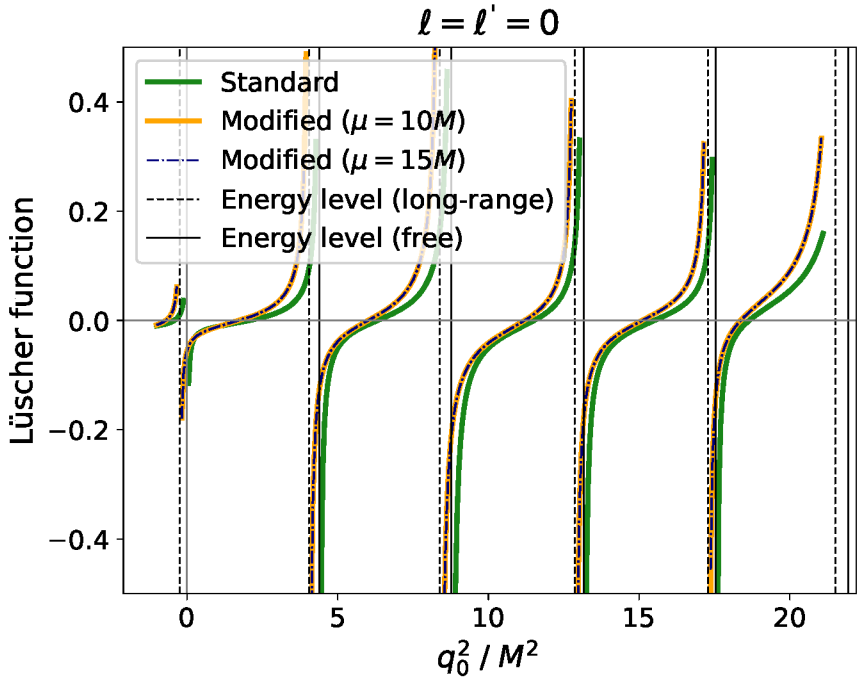

Figure 2. Modified Lüscher zeta-function in the S-wave vs. standard Lüscher zeta-function for two different values of parameter μ: $\mu = 10M$ and $\mu = 15M$. The size of the box is fixed by $ML = 3$. The difference between these two values of μ is not seen by a bare eye.

The key property of this expression is that the quantity G_μ does not have a singular denominator in the physical region. Consequently, $G_\mu - G_\mu^\infty$ is suppressed by factors of $\exp(-\mu L)$ and can be safely neglected.[3] After dropping $G_\mu - G_\mu^\infty$, the remainder contains the subtracted propagator G_f only and is ultraviolet-finite both in a finite and in the infinite volume separately. In this manner, the quantity ΔH can be straightforwardly evaluated using numerical methods. Ultraviolet divergences are absent. No partial-wave expansion is involved for the long-range potential, and the Lippmann-Schwinger equation in a finite volume is solved in a plane-wave basis.

In figure 2 and 3 we plot the modified Lüscher zeta-function[4] $H^\Gamma_{t\ell,t'\ell'}(q_0)$ (see eq. (3.1)) vs. the standard Lüscher zeta-function obtained from $H^\Gamma_{t\ell,t'\ell'}(q_0)$ at $g = 0$. The angular momenta take the values $\ell, \ell' = 0, 4$, and $q_0^2 = E/M$. The labels t, t' are neglected, because multiple representations are not present. The calculations of the modified Lüscher zeta-function are done for two different values of the parameter μ. As seen from figure 2, the results are practically independent of μ, which serves as a very good check on the calculations.

The calculated modified and standard functions are very similar to each other, except for a small horizontal shift. A difference, however, emerges in the vicinity of the lowest energy level corresponding to the relative momentum $\boldsymbol{p} = (0, 0, 0)$: except in the case $\ell = \ell' = 0$, the

[3] A warning is in order: for certain values of the parameters, the quantities G_μ and G_f can develop subthreshold poles that cancel in the sum. However, one can always adjust the free parameter μ, so that these poles lie far outside the region of interest.

[4] Strictly speaking, $H^\Gamma_{t\ell,t'\ell'}(q_0)$ in the free case is given by a linear combination of the zeta-functions with known group-theoretical coefficients. For brevity, we shall refer to $H^\Gamma_{t\ell,t'\ell'}(q_0)$ as the zeta-function as well.

JHEP10(2025)197

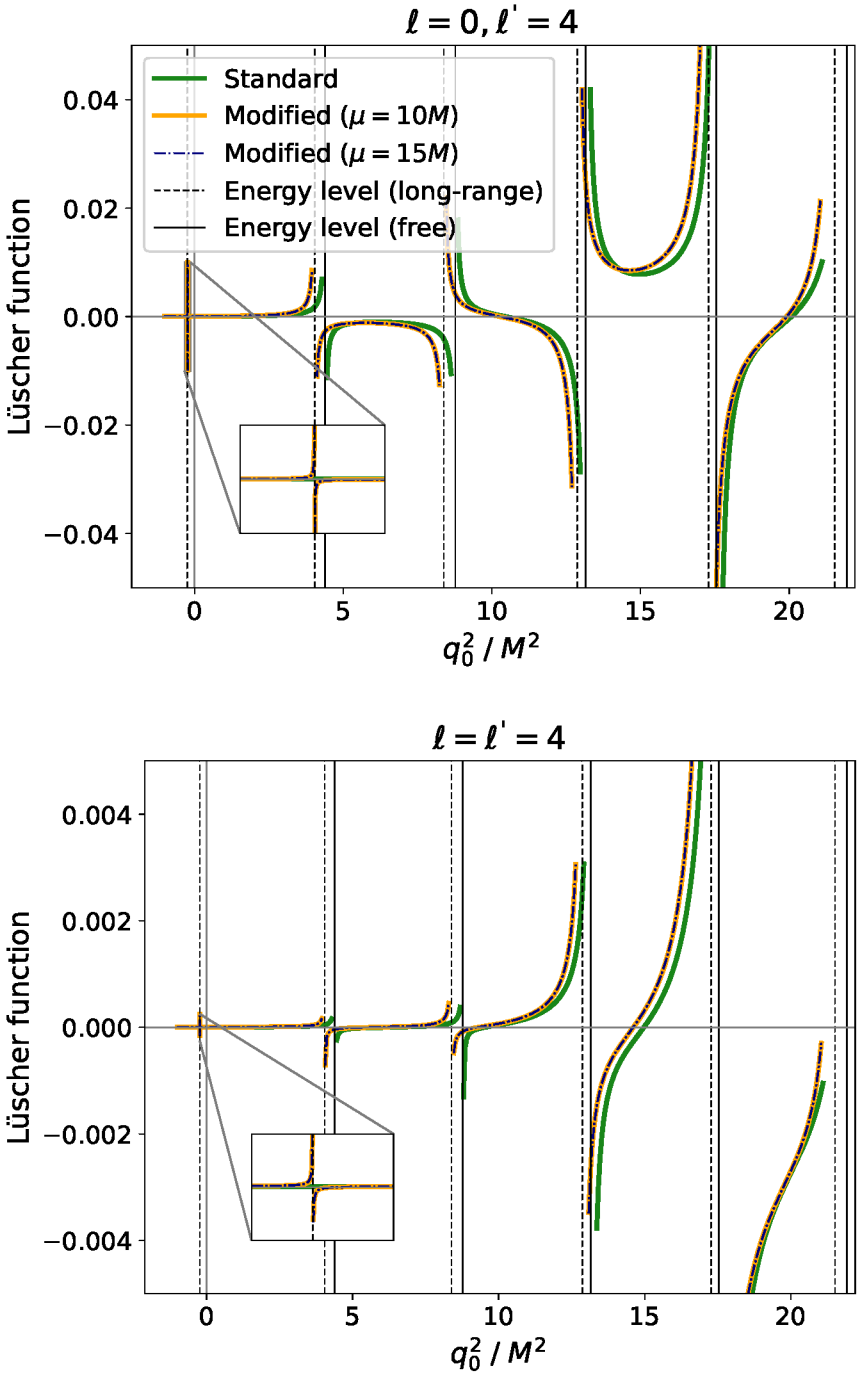

Figure 3. The same as in figure 2, but for higher partial-waves. The vicinity of the lowest energy level is zoomed. Here, the modified function, unlike the standard one, has a pole.

JHEP10(2025)197

standard Lüscher zeta-function does not have a pole here. However, the modified function is a solution of the Lippmann-Schwinger type equation, where all momenta are present in the intermediate state, and therefore it develops a pole at the energy corresponding to the lowest level. For a better visibility, the singular behavior of the modified Lüscher zeta-function in this energy region is zoomed in for the cases $\ell = 0, \ell' = 4$ and $\ell = \ell' = 4$.

3.2 Analysis of the synthetic data

The potential of the toy model, which are used to produce the synthetic lattice data, is given by a sum of the long- and short-range parts:

$$V(\boldsymbol{p}, \boldsymbol{q}) = \frac{4\pi g}{M^2 + (\boldsymbol{p} - \boldsymbol{q})^2} + \frac{4\pi g_S}{M_S^2 + (\boldsymbol{p} - \boldsymbol{q})^2}\,, \tag{3.10}$$

with $g_S/g = -2.74$. In addition, we set the ratio $m/M = 6.7$. Moreover, we treat M_S/M as a free parameter, in order to observe a smooth transition from the short-range to the long-range interaction.

First of all, note that one can easily solve the finite-volume quantization condition with the above potential, finding the eigenvalues of the Hamiltonian in the plane-wave basis. These solutions will be used to test the validity of our method, since both approaches coincide up to the exponentially small corrections. Note also that, in the Hamiltonian approach, one can mimic the truncation of higher partial waves in the Lüscher equation. To this end, one has merely to project the input potential onto the partial waves and drop higher partial waves in this projection.

As we know, one of the fundamental problems in using the Lüscher equation in the presence of a long-range force consists in a slow convergence of the partial-wave expansion. In order to compare the convergence speed in case of the standard/modified Lüscher approach, we retain only S- and G-waves in the quantization condition. The equation (3.4) then yields

$$D(E) = \left(\frac{1}{4\pi}\, K_0^M(q_0) - H_{00}(q_0)\right) - \frac{(H_{04}(q_0))^2}{\left(\frac{1}{4\pi}\, K_4^M(q_0) - H_{44}(q_0)\right)} = 0\,. \tag{3.11}$$

Here the labels t, t' are omitted for brevity. In case of the standard Lüscher equation, $K_\ell^M(q_0)$ is replaced by $K_\ell(q_0)$, and $H_{\ell\ell'}(q_0)$ by the expression evaluated at $g = 0$. If only the S-wave is taken into account, the second term in the expression (3.11) is dropped. Calculations are done for two values $M_S/M = 10$ and $M_S/M = 2$, corresponding to the two extreme cases.

Let us start with the excited states. The solutions of the quantization condition for the first few excited levels and for $M_S/M = 10$ are seen in figure 4. This plot beautifully demonstrates the advantage of the modified quantization condition with respect to the standard one. Namely, while taking into account the partial waves with $\ell = 0, 4, \ldots$, the solution of the standard Lüscher equation slowly converges to the exact solution. In contrast, the solution of the modified quantization condition with the S-wave only already reproduces the exact energy level, and adding the G-wave does not change anything — the two curves cannot be distinguished from each other.

The pattern, described above, remains practically unchanged in case of $M_S/M = 2$, shown in figure 5, which describes a borderline situation with V_S almost long-range. Now, adding

JHEP10(2025)197

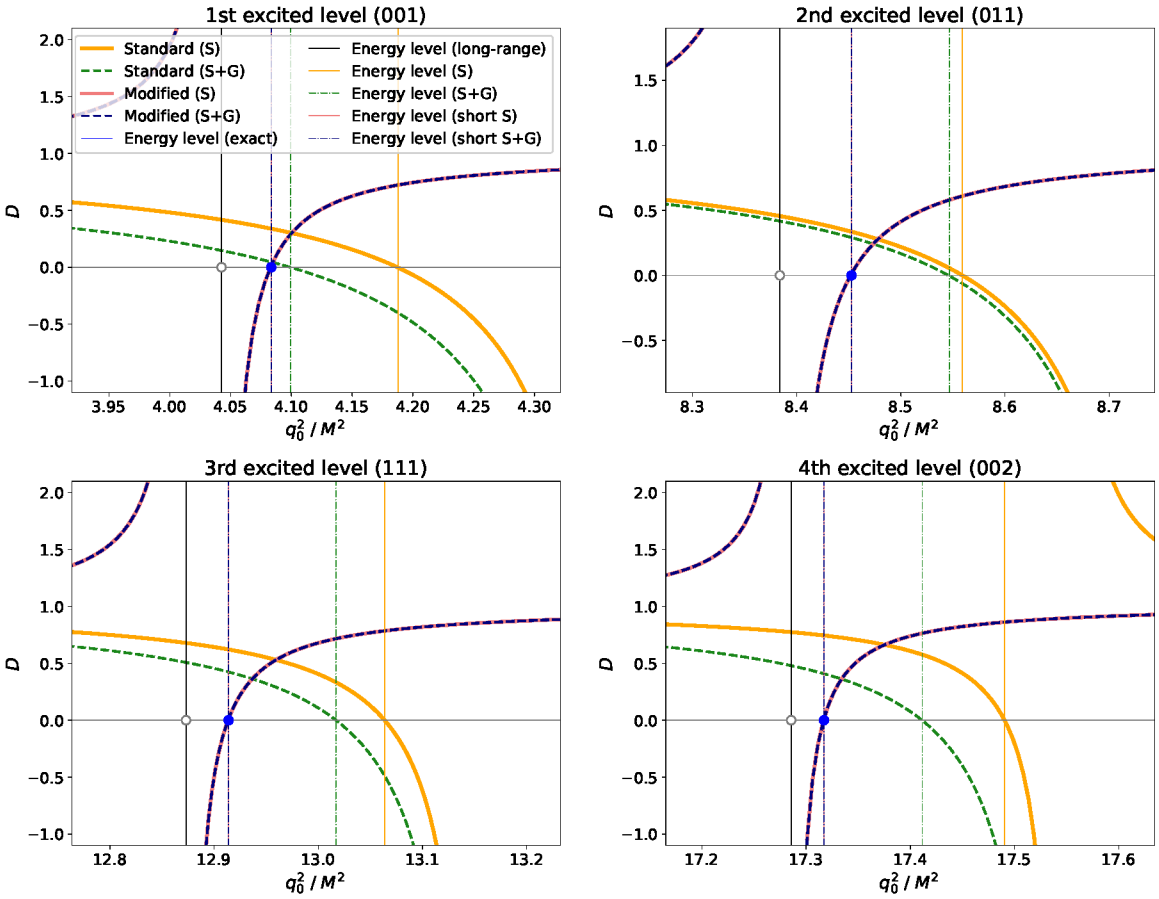

Figure 4. The solution of the quantization condition for the first few excited levels (both the standard and modified Lüscher equation). The partial-wave expansion is truncated, retaining only S-wave, or S- and G-waves. For comparison, the eigenvalues of the Hamiltonian are shown by vertical lines: exact, projected on S, S+G waves, only the short-range part projected on S, S+G waves. In addition, we show a solution with the long-range potential only, i.e., $V_S = 0$. The values of the parameters used are $M_S = 10M$, $ML = 3$. In the title of each plot, we indicate an unperturbed plane-wave state momentum, to which this state reduces in the absence of the interaction.

the G-wave leads to a visible effect, but still the convergence of the modified quantization condition is much better as compared to the standard one.

Few comments are in order. First, as seen, the exponentially suppressed effects are very small, because the solutions of the quantization condition reproduce very well the finite-volume spectrum of the Hamiltonian in the plane-wave basis. Second, the convergence of the partial-wave expansion is rather uneven. This can be seen better from figure 6 and 7, which shows the finite-volume spectrum of the Hamiltonian with the full potential projected onto different partial waves. As seen, for example, the contribution of the G-wave to the 2nd excited state is rather small, and the higher partial waves contribute significantly. A qualitative discussion of this phenomenon is given in appendix A. In general, as expected, the convergence becomes slower for higher partial waves, with relative momentum increased.

JHEP10(2025)197

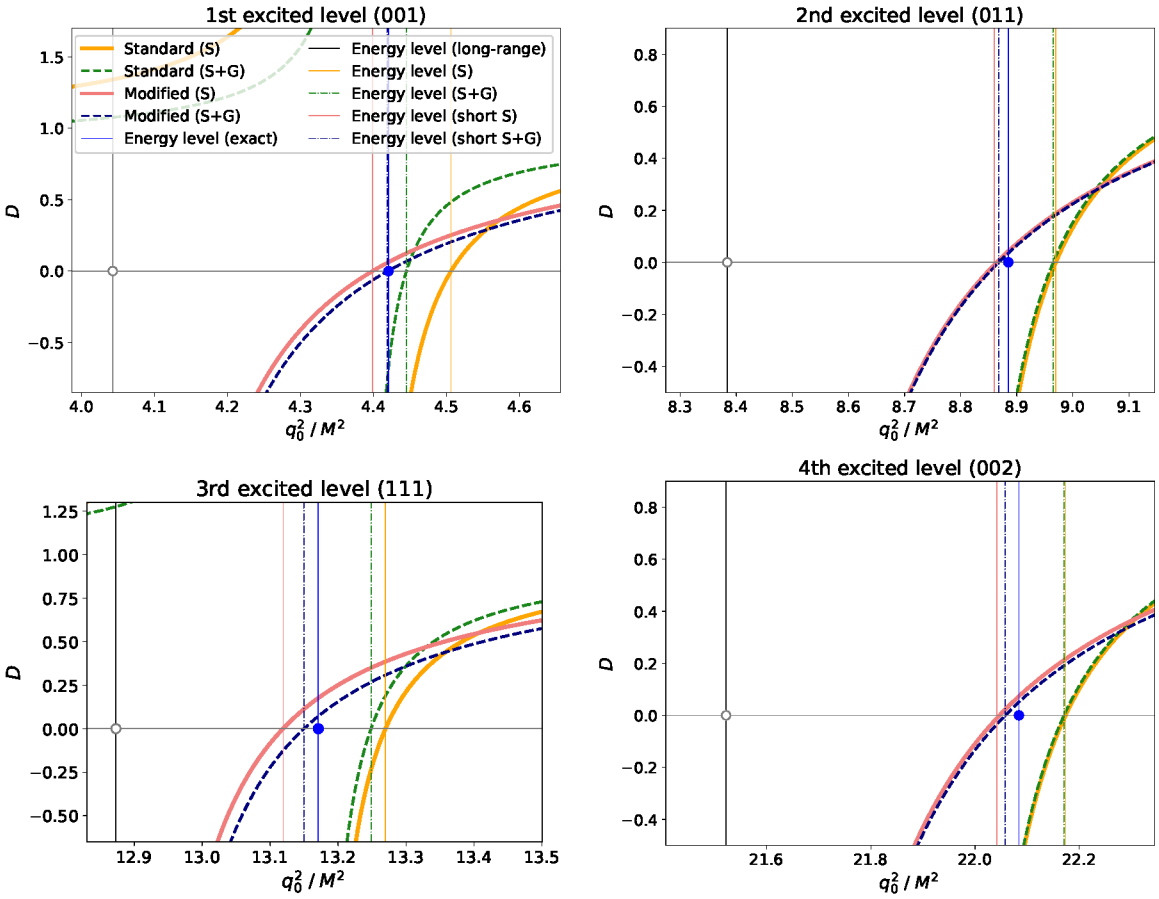

Figure 5. The same as in figure 4, but for $M_S = 2M$.

Last but not least, we would like to note that in the situation when the short-range is completely absent (i.e., when $V_S = 0$), the energy levels are given by the poles of the modified Lüscher zeta-function $H_{\ell\ell'}(q_0)$. In figures 4 and 5, these poles are indicated by empty circles. It is seen that, even for $M_S = 10M$, the effect of setting $V_S = 0$ is sizable. However,the S-wave contribution alone suffices to reproduce the exact answer. This means that the partial-wave expansion in the modified Lüscher equation converges very fast indeed, and the truncation to the S-wave yields a very good approximation, in difference to the standard approach.

The ground state is considered separately. First, note that the convergence of the partial-wave expansion in the Hamiltonian approach is very good,[5] see figure 6, even for the standard case. The solution of the quantization condition, however, shown in figure 8 presents different picture. The modified quantization condition still provides a very accurate solution at $M_S/M = 10$ and a quite accurate solution at $M_S/M = 2$. The standard Lüscher equation, however, is completely off. The reason for this is the proximity of the left-hand cut which leads to large exponential corrections. As expected, these corrections are strongly suppressed in the modified quantization condition as compared to the standard one.

[5]It is worth to mention that for some particular excited state, the G-wave contribution is obviously suppressed, for example, the 2nd excited level which is around the momentum of $(0, 1, 1)$. A detailed discussion is presented in appendix A.

JHEP10(2025)197

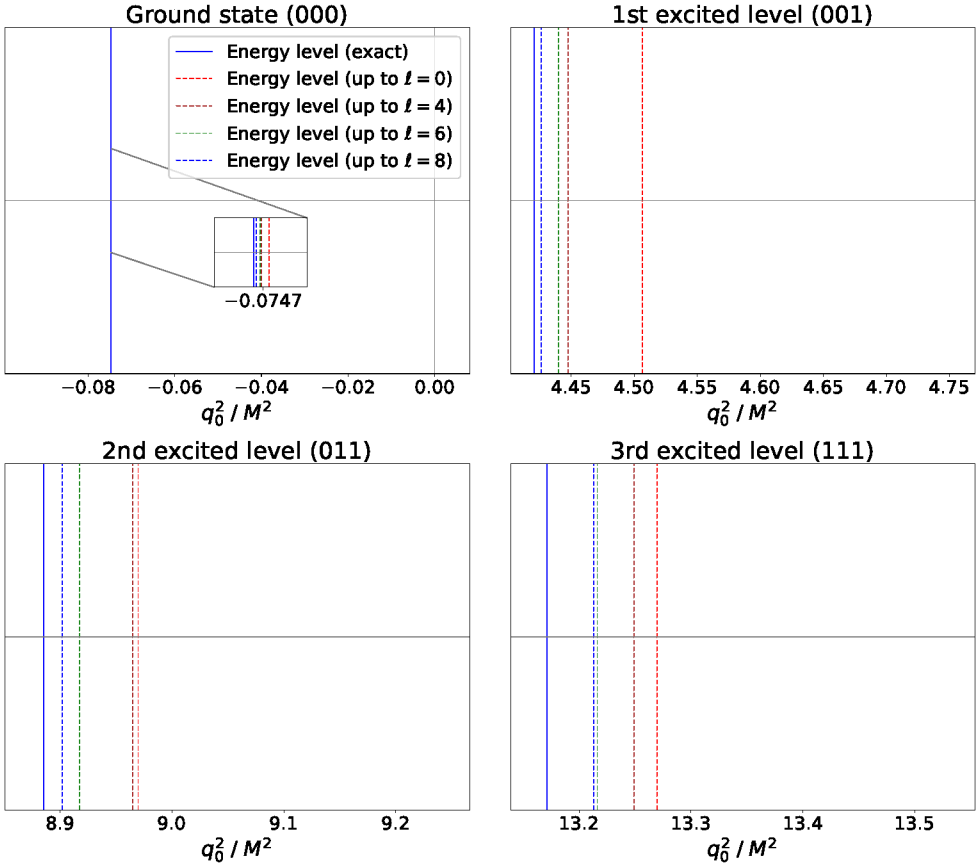

Figure 6. Checking the convergence of the partial-wave expansion in the energy spectrum of the Hamiltonian. The values of the parameters used are $M_S = 10M$ and $ML = 3$.

In order to understand this result qualitatively, let us introduce a characteristic parameter that determines, how far the left-hand cut is located from a given energy level. In the case of standard and modified Lüscher equations, the left-hand cut starts at $q_0^2/M^2 = -1/4$ and $q_0^2/M^2 = -M_S^2/4M^2$, respectively. If one divides this quantity by the value of q_0^2/M^2 corresponding to the ground state (taken from the figure) and extracts the square root, one ends up with a ratio of momentum scales. In the case of the standard Lüscher equation, this ratio is equal to 1.1 and 1.9 for $M_S = 10M$ and $M_S = 2M$, respectively. In the modified case, this ratio becomes 11 and 3.8, respectively. This, in our opinion, explains why the exponential corrections in the modified case are much smaller than in the standard setting. It would be interesting to see, which value a similar parameter takes in the analysis of data carried out in ref. [14], since this might provide a rough estimate of the exponential corrections which are neglected in this analysis.

4 Modified effective range expansion in the left-hand cut region

4.1 Calculation of the loop function $M_\ell(q_0)$

The function $M_\ell(q_0)$ is given by eq. (2.5). As already mentioned, this quantity is ultraviolet-divergent. One way to regularize this divergence is to render the long-range potential

JHEP10(2025)197

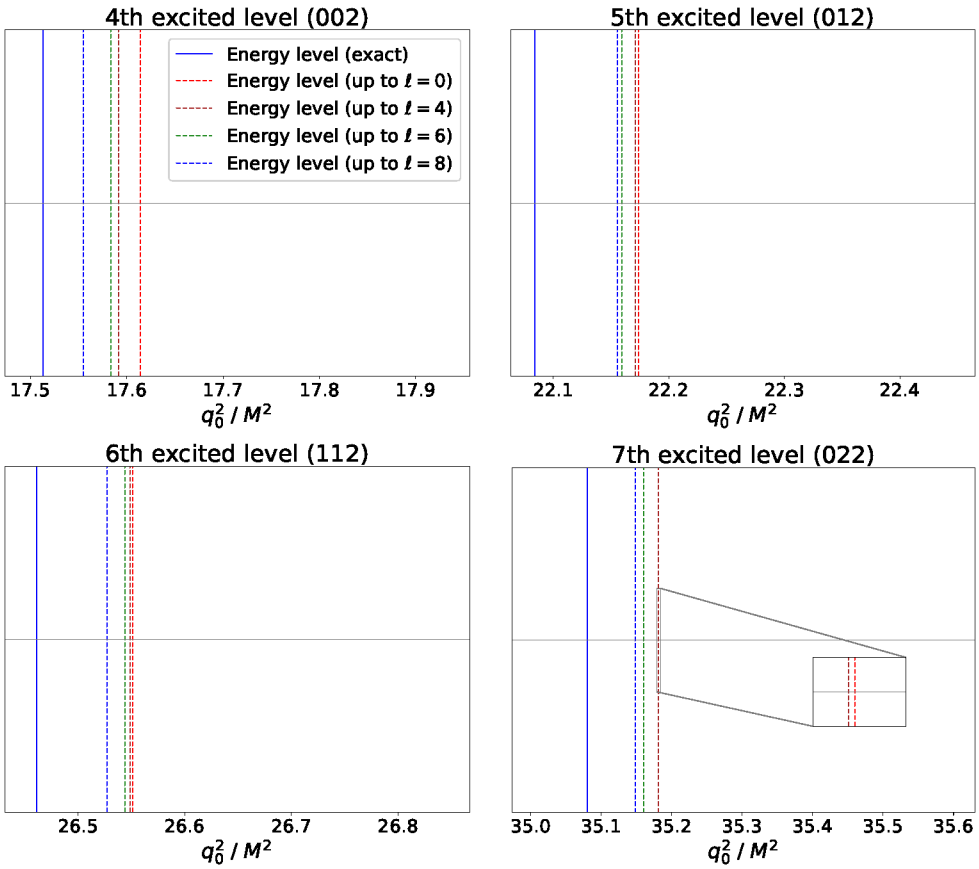

Figure 7. The same as in figure 6, but for higher excited states.

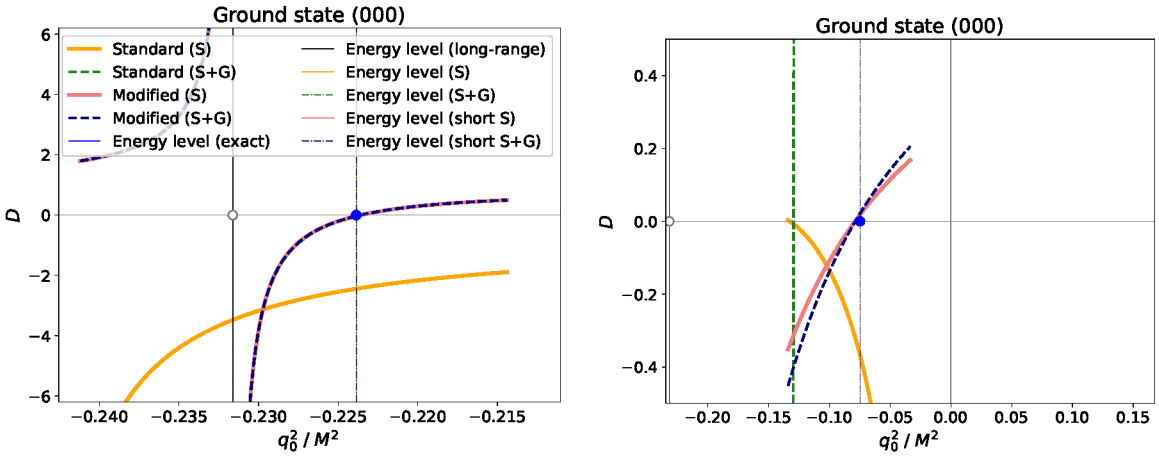

Figure 8. The solution of the quantization condition (both standard and modified) for the ground state. The values of the parameters are $ML = 3$ and $M_S = 10M$ (left panel), $M_S = 2M$ (right panel). There is no solution of the standard quantization condition in case $M_S = 10M$.

JHEP10(2025)197

superregular, e.g., by using the Pauli-Villars regularization or a sharp cutoff. The price to pay for using this straightforward procedure is that the coefficients of the modified effective range expansion if the function $K_\ell^M(q_0^2)$ are not of natural size anymore. Indeed, let Λ denote the (large) cutoff mass used in the regularization. For a given ℓ, the loop diverges as $\Lambda^{2\ell+1}$. Since in the modified effective range expansion this loop enters in a combination $K_\ell^M(q_0^2) - M_\ell(q_0)$, it is clear that this polynomial with large coefficients has to be absorbed into $K_\ell^M(q_0^2)$. At the practical level, the cutoff regularization becomes numerically inconvenient for even not so large values of ℓ.[6] For this reason, we propose to use dimensional regularization instead, where the power divergences are absent. However, in this case, we encounter another problem. Namely, the quantity $G_L(q_0)$, which enters the expression for $M_\ell(q_0)$, contains an infinite sum of one-pion exchange ladder diagrams (see figure 1) and is determined through the solution of an integral equation. It is not obvious how one can use dimensional regularization to tame divergences in the integral equation.

The key observation that allows one to solve the problem is that each consequent term in the Born series of $G_L(q_0)$ has a lower index of divergence than the previous one. Therefore, only a finite number of terms in the expansion diverge. One can use this property and split $G_L(q_0)$ into two parts: $G_L(q_0) = G_L^{\mathsf{div}}(q_0) + G_0(q_0)T_L^{\mathsf{fin}}G_0(q_0)$, and, correspondingly, $M_\ell(q_0) = M_\ell^{\mathsf{div}}(q_0) + M_\ell^{\mathsf{fin}}(q_0)$, where

$$\begin{aligned} G_L^{\mathsf{div}}(q_0) &= \underbrace{\left(G_0(q_0) + G_0(q_0)V_L G_0(q_0) + \cdots\right)}_{2\ell+2 \text{ terms}}, \\ T_L^{\mathsf{fin}} &= \underbrace{\left(V_L + V_L G_0(q_0) V_L + \cdots\right)}_{2\ell+2 \text{ terms}} + V_L G_0(q_0) T_L^{\mathsf{fin}}. \end{aligned} \tag{4.1}$$

The integral equation that determines T_L^{fin} is of a Lippmann-Schwinger type and can be numerically solved by using standard techniques. The loop integral, containing T_L^{fin}, is free of ultraviolet divergences. Hence all calculations can be carried out in $d = 3$ dimensions.

The remainder is given by the following expression:

$$M_\ell^{\mathsf{div}}(q_0) = 4\pi \int \frac{d^3\boldsymbol{p}}{(2\pi)^3} \frac{d^3\boldsymbol{q}}{(2\pi)^3} (pq)^\ell P_\ell(\hat{p}\cdot\hat{q}) \langle \boldsymbol{p}| G_L^{\mathsf{div}}(q_0) |\boldsymbol{q}\rangle . \tag{4.2}$$

In order to carry out dimensional regularization in the above expression, one should first define Legendre polynomials $P_\ell(x)$ in d dimensions. This definition is not unique. However, using different definitions reduces to adding a finite polynomial in q_0^2 to $M_\ell^{\mathsf{div}}(q_0)$ and hence can be accounted for by adjusting the renormalization prescription. Our definition is based on the use of the d-dimensional harmonic polynomials $\mathscr{Y}^{(\ell)}_{i_1\cdots i_\ell}(\boldsymbol{p}) = y_{i_1\cdots i_\ell, j_1\cdots j_\ell} p_{j_1}\cdots p_{j_\ell}$, which have the following properties:

- $\mathscr{Y}^{(\ell)}_{i_1\cdots i_\ell}(\boldsymbol{p})$ is a polynomial in the components of the vector $\boldsymbol{p}$;
- $\mathscr{Y}^{(\ell)}_{i_1\cdots i_\ell}(\boldsymbol{p})$ is symmetric and traceless in any pair of indices.

[6] It should be mentioned that the problem of the ultraviolet divergences in the modified effective range expansion has been observed in the literature before, see, e.g., ref. [27].

JHEP10(2025)197

The examples of harmonic polynomials for $\ell = 0, 1, 2, 3, 4$ are given below:

$$\begin{aligned}
\mathscr{Y}^{(0)}(\boldsymbol{p}) &= 1\,,\\
\mathscr{Y}^{(1)}_i(\boldsymbol{p}) &= p_i\,,\\
\mathscr{Y}^{(2)}_{ij}(\boldsymbol{p}) &= p_ip_j - \frac{1}{d}\,\boldsymbol{p}^2\,,\\
\mathscr{Y}^{(3)}_{ijk}(\boldsymbol{p}) &= p_ip_jp_k - \frac{1}{d+2}\,\boldsymbol{p}^2(\delta_{ij}p_k + \delta_{ik}p_j + \delta_{jk}p_i)\,,\\
\mathscr{Y}^{(4)}_{ijkl}(\boldsymbol{p}) &= p_ip_jp_kp_l - \frac{1}{d+4}\,\boldsymbol{p}^2(\delta_{ij}p_kp_l + \delta_{ik}p_jp_l + \delta_{il}p_jp_k + \delta_{jk}p_ip_l + \delta_{jl}p_ip_k + \delta_{kl}p_ip_j)\\
&\quad + \frac{1}{(d+2)(d+4)}\,\boldsymbol{p}^4(\delta_{ij}\delta_{kl} + \delta_{ik}\delta_{jl} + \delta_{il}\delta_{jk})\,,
\end{aligned} \tag{4.3}$$

and so on. The coefficients $y_{i_1\cdots i_\ell, j_1\cdots j_\ell}$ can be easily read off from these expressions. Furthermore,

$$(pq)^\ell P_\ell(\hat{p}\cdot\hat{q}) = c_d^{(\ell)} \sum_{i_i,\cdots,i_\ell} \mathscr{Y}^{(\ell)}_{i_1\cdots i_\ell}(\boldsymbol{p})\mathscr{Y}^{(\ell)}_{i_1\cdots i_\ell}(\boldsymbol{q})\,. \tag{4.4}$$

This gives

$$\begin{aligned}
P_0(\hat{p}\cdot\hat{q}) &= 1\,,\\
(pq)P_1(\hat{p}\cdot\hat{q}) &= (\boldsymbol{pq})\,,\\
(pq)^2P_2(\hat{p}\cdot\hat{q}) &= \frac{d}{d-1}\left((\boldsymbol{pq})^2 - \frac{1}{d}\,\boldsymbol{p}^2\boldsymbol{q}^2\right)\,,\\
(pq)^3P_3(\hat{p}\cdot\hat{q}) &= \frac{d+2}{d-1}\left((\boldsymbol{pq})^3 - \frac{3}{d+2}\,(\boldsymbol{pq})\boldsymbol{p}^2\boldsymbol{q}^2\right)\,,\\
(pq)^4P_4(\hat{p}\cdot\hat{q}) &= \frac{(d+2)(d+4)}{d^2-1}\left((\boldsymbol{pq})^4 - \frac{6}{d+4}\,(\boldsymbol{pq})^2\boldsymbol{p}^2\boldsymbol{q}^2 + \frac{3}{(d+2)(d+4)}\,\boldsymbol{p}^4\boldsymbol{q}^4\right)\,,
\end{aligned} \tag{4.5}$$

and so on. The normalization constant $c_d^{(\ell)}$ is chosen so that $P_\ell(1) = 1$ for all d.

Since our calculations are restricted to the A_1^+ irrep of the octahedral group for demonstration purposes, it suffices to consider the angular momenta $\ell = 0, 4$.

4.1.1 The case $\ell = 0$

In this case, only the two-loop diagram $M^{\mathsf{div}}_{0,2}(q_0)$ (the second diagram in figure 1) should be considered. The one-loop diagram with no pion exchange can be easily evaluated in dimensional regularization and the rest is ultraviolet-finite. The two-loop diagram in dimensional regularization is given by

$$\begin{aligned}
M^{\mathsf{div}}_{0,2}(q_0) &= 4\pi \int \frac{d^d\boldsymbol{p}}{(2\pi)^d}\,\frac{d^d\boldsymbol{q}}{(2\pi)^d}\,\frac{1}{\boldsymbol{p}^2 - q_0^2}\,\frac{4\pi g}{M^2 + (\boldsymbol{p}-\boldsymbol{q})^2}\,\frac{1}{\boldsymbol{q}^2 - q_0^2}\\
&= \int_0^1 \mathscr{D}_{xy} \int \frac{d^d\boldsymbol{p}}{(2\pi)^d}\,\frac{d^d\boldsymbol{q}}{(2\pi)^d}\,\frac{\Gamma(3)\,(4\pi)^2 g}{\left(x_1(\boldsymbol{p}^2 - q_0^2) + y(M^2 + (\boldsymbol{p}-\boldsymbol{q})^2) + x_2(\boldsymbol{q}^2 - q_0^2)\right)^3}\,,
\end{aligned} \tag{4.6}$$

where

$$\mathscr{D}_{xy} = dx_1dx_2dy\,\delta(1 - x_1 - x_2 - y)\,. \tag{4.7}$$

JHEP10(2025)197

One can rewrite the above expression in a compact form, introducing a 2-dimensional column $\boldsymbol{Q}_\alpha$, $\alpha = 1, 2$, where $\boldsymbol{Q}_1 = \boldsymbol{p}$ and $\boldsymbol{Q}_2 = \boldsymbol{q}$. Then,

$$M_{0,2}^{\mathsf{div}}(q_0) = \int_0^1 \mathscr{D}_{xy} \int \frac{d^{2d}\boldsymbol{Q}}{(2\pi)^{2d}} \frac{\Gamma(3)\,(4\pi)^2 g}{\left(\sum\limits_{\alpha,\beta} \boldsymbol{Q}_\alpha C_{\alpha\beta} \boldsymbol{Q}_\beta + \Delta\right)^3}\,, \tag{4.8}$$

where

$$C = \begin{pmatrix} x_1 + y & -y \\ -y & y + x_2 \end{pmatrix}\,, \qquad \Delta = yM^2 - (x_1 + x_2)q_0^2\,. \tag{4.9}$$

One can now perform orthogonal transformations in order to diagonalize the matrix C. The result looks as

$$M_{0,2}^{\mathsf{div}}(q_0) = \int_0^1 \mathscr{D}_{xy} \int \frac{d^{2d}\boldsymbol{Q}}{(2\pi)^{2d}} \frac{\Gamma(3)\,(4\pi)^2 g}{\left(\sum\limits_{\alpha} \boldsymbol{Q}_\alpha \lambda_\alpha \boldsymbol{Q}_\alpha + \Delta\right)^3}\,, \tag{4.10}$$

where λ_α denote the eigenvalues of the matrix C. Rescaling further the momenta $\boldsymbol{Q}_\alpha \to \lambda_\alpha^{-1/2} \boldsymbol{Q}_\alpha$, we get:

$$\begin{aligned} M_{0,2}^{\mathsf{div}}(q_0) &= \int_0^1 \mathscr{D}_{xy} \int \frac{d^{2d}\boldsymbol{Q}}{(2\pi)^{2d}} \frac{\Gamma(3)\,(4\pi)^2 g \det(C)^{-d/2}}{\left(\sum\limits_{\alpha} \boldsymbol{Q}_\alpha \boldsymbol{Q}_\alpha + \Delta\right)^3} \\ &= \frac{\Gamma(3-d) g}{(4\pi)^{d-2}} \int_0^1 \mathscr{D}_{xy} \det(C)^{-d/2} \Delta^{d-3}\,. \end{aligned} \tag{4.11}$$

We further introduce the new variables $x_1 = \rho\tau$ and $x_2 = \rho(1-\tau)$, with $0 \le \rho, \tau \le 1$. Defining the dimensionless quantity $z = q_0^2/M^2$ and carrying out the integration in y, we get

$$\begin{aligned} M_{0,2}^{\mathsf{div}}(q_0) &= \frac{\Gamma(3-d) g (M^2)^{d-3}}{(4\pi)^{d-2}} \int_0^1 \rho d\rho d\tau ((1-\rho) - \rho z)^{d-3} (\rho(1-\rho) + \rho^2 \tau(1-\tau))^{-d/2} \\ &= \frac{\Gamma(3-d) g (M^2)^{d-3}}{(4\pi)^{d-2}} \int_0^\infty ds \int_0^1 d\tau (s - z)^{d-3} (s + \tau(1-\tau))^{-d/2} \\ &= -\frac{g}{2(d-3)} + \text{UV finite}, \end{aligned} \tag{4.12}$$

where a new integration variable $s = (1-\rho)/\rho$ was introduced.

As anticipated, the two-loop diagram is ultraviolet divergent. One could use, for example, MS or $\overline{\text{MS}}$ renormalization scheme, using M (as the only available mass) as a renormalization scale. The advantage of such a procedure consists in the fact that no large polynomials should be absorbed in $K_\ell^M(q_0^2)$ anymore. It should be pointed, however, that using this scheme becomes more complicated for higher values of ℓ, even if the above statement still applies. Namely, there are more divergent diagrams for higher ℓ, and the factors $(d-3)^{-1}$ may arise either from the prefactor containing the Γ-function, or the integral over the variable s, and the separation of the all ultraviolet-divergent terms becomes involved. We find that a simple solution to the problem is to impose a different renormalization prescription, namely,

JHEP10(2025)197

to subtract first few terms in the Taylor expansion at threshold $z = 0$. In the case we are considering, a single subtraction suffices, since the divergent term is a constant:

$$\hat{M}^{\mathsf{div}}_{0,2}(q_0) = M^{\mathsf{div}}_{0,2}(q_0) - M^{\mathsf{div}}_{0,2}(0)\,. \tag{4.13}$$

For higher ℓ, more subtractions are necessary.

4.1.2 The case $\ell = 4$

In the section above we have considered the case $\ell = 0$ in great detail, including the discussion of the ultraviolet regularization and the choice of the renormalization prescription. Most of the techniques, used here, can be applied for higher values of ℓ without change. In this case, however, there are more divergent diagrams. The N-loop diagram can be written as follows:

$$\begin{aligned} M^{\mathsf{div}}_{4,N}(q_0) &= 4\pi \int \frac{d^d\boldsymbol{Q}_1}{(2\pi)^d} \cdots \frac{d^d\boldsymbol{Q}_N}{(2\pi)^d}\, \frac{1}{\boldsymbol{Q}_1^2 - q_0^2}\, \frac{4\pi g}{M^2 + (\boldsymbol{Q}_1 - \boldsymbol{Q}_2)^2} \cdots \frac{(Q_1Q_N)^4 P_4(\hat{Q}_1 \cdot \hat{Q}_N)}{\boldsymbol{Q}_N^2 - q_0^2} \\ &= \int_0^1 \mathscr{D}_{xy} \int \frac{d^d\boldsymbol{Q}_1}{(2\pi)^d} \cdots \frac{d^d\boldsymbol{Q}_N}{(2\pi)^d}\, \frac{h_N (Q_1Q_N)^4 P_4(\hat{Q}_1 \cdot \hat{Q}_N)}{D^{2N-1}}\,, \end{aligned} \tag{4.14}$$

where $h_N = \Gamma(2N-1)\,(4\pi)^N g^{N-1}$ and

$$D = x_1(\boldsymbol{Q}_1^2 - q_0^2) + y_1(M^2 + (\boldsymbol{Q}_1 - \boldsymbol{Q}_2)^2) + \cdots + x_N(\boldsymbol{Q}_N^2 - q_0^2)\,. \tag{4.15}$$

Here, the Feynman parameters x_i, $i = 1, \ldots, N$ and $y_i, i = 1, \ldots, N-1$ are associated with the Green function $(\boldsymbol{Q}_i^2 - q_0^2)^{-1}$ and the pion propagator $(M^2 + (\boldsymbol{Q}_i - \boldsymbol{Q}_{i+1})^2)^{-1}$, respectively, and $\mathscr{D}_{xy} = dx_1 \cdots dx_N dy_1 \cdots dy_{N-1} \delta(1 - x_1 - \cdots - x_N - y_1 - \cdots - y_{N-1})$. The tridiagonal matrix C takes the following form

$$C = \begin{pmatrix} x_1 + y_1 & -y_1 & 0 & 0 & 0 & \cdots & 0 \\ -y_1 & x_2 + y_1 + y_2 & -y_2 & 0 & 0 & \cdots & 0 \\ 0 & -y_2 & x_3 + y_2 + y_3 & -y_3 & 0 & \cdots & 0 \\ & & \cdots & & & & -y_{N-1} \\ 0 & \cdots & 0 & 0 & 0 & -y_{N-1} & x_N + y_{N-1} \end{pmatrix} \tag{4.16}$$

Let the matrix O be an orthogonal matrix that diagonalizes C: $(OCO^T)_{\alpha\beta} = \lambda_\alpha \delta_{\alpha\beta}$. The variable transformation $\boldsymbol{Q}_\alpha \to O_{\alpha\beta}\lambda_\beta^{-1/2}\boldsymbol{Q}_\beta$ transforms the denominator into

$$D \to \sum_\alpha \boldsymbol{Q}_\alpha \boldsymbol{Q}_\alpha + \Delta, \qquad \Delta = (y_1 + \cdots + y_{N-1})M^2 - (x_1 + \cdots + x_N)q_0^2\,. \tag{4.17}$$

The multi-loop integral is then rewritten in the following form:

$$M^{\mathsf{div}}_{4,N}(q_0) = \int_0^1 \mathscr{D}_{xy} \int \frac{d^{Nd}\boldsymbol{Q}}{(2\pi)^{Nd}}\, \frac{\det(C)^{-d/2} h_N c_d^{(4)}}{D^{2N-1}} \left(N_4 - \frac{6}{d+4}\, N_2 + \frac{3}{(d+2)(d+4)}\, N_0\right). \tag{4.18}$$

In order to simplify notations, we further introduce the multiindex $A = (\alpha, i)$ and $B = (\beta, j)$. Here $\alpha, \beta = 1, \ldots N$ and $i, j = 1, 2, 3$ label the loop momentum and the space index of the Nd-dimensional vector $\boldsymbol{Q} = (\boldsymbol{Q}_1, \cdots, \boldsymbol{Q}_N)$. We further define $v_\alpha^{(1)} = O_{1\alpha}\lambda_\alpha^{-1/2}$ and

$v_\beta^{(N)} = O_{1\beta}\lambda_\beta^{-1/2}$. The terms in the numerator of the Feynman integral can be written in the following compact notation ($K = 0, 2, 4$)

$$N_K = v_{\alpha_1}^{(1)} \cdots v_{\alpha_4}^{(1)}\, v_{\beta_1}^{(N)} \cdots v_{\beta_4}^{(N)}\, \Phi^{(K)}_{i_1\cdots i_4, j_1\cdots j_4}\, Q_{A_1}\cdots Q_{A_4} Q_{B_1}\cdots Q_{B_4}\,, \tag{4.19}$$

where

$$\begin{aligned}
\Phi^{(0)}_{i_1\cdots i_4, j_1\cdots j_4} &= \delta_{i_1 i_2}\delta_{i_3 i_4}\delta_{j_1 j_2}\delta_{j_3 j_4}\,,\\
\Phi^{(2)}_{i_1\cdots i_4, j_1\cdots j_4} &= \delta_{i_1 i_2}\delta_{j_1 j_2}\delta_{i_3 j_3}\delta_{i_4 j_4}\,,\\
\Phi^{(4)}_{i_1\cdots i_4, j_1\cdots j_4} &= \delta_{i_1 j_1}\delta_{i_2 j_2}\delta_{i_3 j_3}\delta_{i_4 j_4}\,.
\end{aligned} \tag{4.20}$$

Since the denominator of the Feynman integral depends only on the Nd-dimensional vector squared, it is possible to average over the directions. We define

$$\begin{aligned}
\langle Q_A Q_B\rangle &= a_1\, Q^2\, \Pi^{(1)}_{AB}\,,\\
\langle Q_{A_1} Q_{A_2} Q_{B_1} Q_{B_2}\rangle &= a_2\, Q^4\, \Pi^{(2)}_{A_1A_2B_1B_2}\,,\\
\langle Q_{A_1} Q_{A_2} Q_{A_3} Q_{B_1} Q_{B_2} Q_{B_3}\rangle &= a_3\, Q^6\, \Pi^{(3)}_{A_1A_2A_3B_1B_2B_3}\,,\\
\langle Q_{A_1} Q_{A_2} Q_{A_3} Q_{A_4} Q_{B_1} Q_{B_2} Q_{B_3} Q_{B_4}\rangle &= a_4\, Q^8\, \Pi^{(4)}_{A_1A_2A_3A_4B_1B_2B_3B_4}\,.
\end{aligned} \tag{4.21}$$

It is clear that the quantities Π are symmetric with respect to the permutations of any of two indices. Furthermore,

$$\begin{aligned}
\Pi^{(1)}_{AB} &= \delta_{AB}\,,\\
\Pi^{(2)}_{A_1A_2B_1B_2} &= \delta_{A_1A_2}\Pi^{(1)}_{B_1B_2} + \delta_{A_1B_1}\Pi^{(1)}_{A_2B_2} + \delta_{A_1B_2}\Pi^{(1)}_{A_2B_1}\,,\\
\Pi^{(3)}_{A_1A_2A_3B_1B_2B_3} &= \delta_{A_1A_2}\Pi^{(2)}_{A_3B_1B_2B_3} + \delta_{A_1A_3}\Pi^{(2)}_{A_2B_1B_2B_3} + \delta_{A_1B_1}\Pi^{(2)}_{A_2A_3B_2B_3}\\
&\quad + \delta_{A_1B_2}\Pi^{(2)}_{A_2A_3B_1B_3} + \delta_{A_1B_3}\Pi^{(2)}_{A_2A_3B_1B_2}\,,\\
\Pi^{(4)}_{A_1A_2A_3A_4B_1B_2B_3B_4} &= \delta_{A_1A_2}\Pi^{(3)}_{A_3A_4B_1B_2B_3B_4} + \delta_{A_1A_3}\Pi^{(3)}_{A_2A_4B_1B_2B_3B_4}\\
&\quad + \delta_{A_1A_4}\Pi^{(3)}_{A_2A_3B_1B_2B_3B_4} + \delta_{A_1B_1}\Pi^{(3)}_{A_2A_3A_4B_2B_3B_4}\\
&\quad + \delta_{A_1B_2}\Pi^{(3)}_{A_2A_3A_4B_1B_3B_4} + \delta_{A_1B_3}\Pi^{(3)}_{A_2A_3A_4B_1B_2B_4}\\
&\quad + \delta_{A_1B_4}\Pi^{(3)}_{A_2A_3A_4B_1B_2B_3}\,,
\end{aligned} \tag{4.22}$$

and so on. The normalization constants $a_1, \ldots, a_4$ can be easily determined, taking the trace on both sides of eq. (4.21)

$$\begin{aligned}
a_1 &= \frac{1}{dN}\,, \qquad a_2 = \frac{1}{dN(dN+2)}\,, \qquad a_3 = \frac{1}{dN(dN+2)(dN+4)}\,,\\
a_4 &= \frac{1}{dN(dN+2)(dN+4)(dN+6)}\,.
\end{aligned} \tag{4.23}$$

It remains to substitute the above formulae into eq. (4.19) and evaluate the numerator after averaging over the directions. After the lengthy but straightforward calculations we arrive at a compact expression

$$M^{\mathsf{div}}_{4,N}(q_0) = \int_0^1 \mathscr{D}_{xy} \int \frac{d^{Nd}\boldsymbol{Q}}{(2\pi)^{Nd}}\, \frac{\det(C)^{-d/2} h_N c_d^{(4)} a_4\,(d-1)d(d+1)(d+6)\, f_{1N}^4\, Q^8}{(Q^2+\Delta)^{2N-1}}\,, \tag{4.24}$$

where $f_{\alpha\beta}$ denotes the matrix element of C^{-1}:

$$f_{\alpha\beta} = \sum_{\gamma} O_{\alpha\gamma} \lambda_{\gamma}^{-1} O_{\beta\gamma} = \det(C)^{-1} \mathrm{Adj}(C)_{\alpha\beta} \,, \tag{4.25}$$

where $\mathrm{Adj}(C)$ is the adjugate of the matrix C. Carrying out the integration over $\boldsymbol{Q}$, we finally get

$$\begin{aligned} M_{4,N}^{\mathsf{div}}(q_0) = {} & \frac{g^{N-1} c_d^{(4)} a_4}{(4\pi)^{N(d/2-1)}} \frac{\Gamma(Nd/2+4)\Gamma(N(2-d/2)-5)}{\Gamma(Nd/2)} \\ & \times \int_0^1 \mathscr{D}_{xy} \, \det(C)^{-d/2-4} \left(\mathrm{Adj}(C)_{1N}\right)^4 \Delta^{N(d/2-2)+5} \,. \end{aligned} \tag{4.26}$$

In order to carry out integrations, it is convenient to group the variables x_i and y_i separately:

$$\begin{aligned} & x_1 = \rho\tau_1, \qquad x_2 = \rho(1-\tau_1)\tau_2, \qquad \cdots \qquad x_N = \rho(1-\tau_1)\cdots(1-\tau_{N-1}) \,, \\ & y_1 = (1-\rho)t_1, \qquad y_2 = (1-\rho)(1-t_1)t_2, \qquad \cdots \qquad y_{N-1} = (1-\rho)(1-t_1)\cdots(1-t_{N-2}) \,, \\ & s = (1-\rho)/\rho \,. \end{aligned} \tag{4.27}$$

As already mentioned, the quantity $M_{4,N}^{\mathsf{div}}(q_0)$ is ultraviolet divergent. It contains a simple pole in $(d-3)$ to all orders that can emerge in different places. For *even* values of N, the pole emerges in $\Gamma(N(2-d/2)-5)$, whereas the integration over the variable s yields a finite result in dimensional regularization, because the index of divergence is half-integer in $d=3$ dimensions. For *odd* values of N, the prefactor is finite, and the pole emerges from the integration over s. Integrating over the variables τ_i and t_i does not produce any divergences. All diagrams with $N > 10$ are ultraviolet-finite.

Separating the poles in multi-loop diagrams is a rather involved enterprise. On the other hand, applying the subtraction at threshold (or any other point below threshold, with a subtraction scale of order of M) can be done straightforwardly. We shall fix our renormalization prescription by subtracting from the multi-loop diagram the first few terms of the Taylor expansion in the variable $z = q_0^2/M^2$. The polynomial of the fourth order in z should be subtracted for $N=2$, the polynomial of the third order for $N=3,4$, the polynomial of the second order for $N=5,6$, and so on. It is clear that this procedure does not introduce large mass scale and, hence, the coefficients of the modified effective range expansion in $K_\ell^M(q_0^2)$ will be of natural size.

4.2 Results of numerical calculations for $M_\ell(q_0)$

In this section we shall present the results of numerical calculations for $\ell = 0, 4$. After subtracting the ultraviolet divergences, the calculation over Feynman parameters in $d=3$ dimensions were carried by using the VEGAS routine [28, 29]. The Lippmann-Schwinger equation (4.1) that determines T_L^{fin} is discretized on Gaussian mesh points and solved by using matrix inversion.

In figure 9 the real and imaginary parts of the function $M_\ell(q_0)$ for $\ell = 0$ are plotted. The full solution $M_\ell(q_0) = M_\ell^{\mathsf{div}}(q_0) + M_\ell^{\mathsf{fin}}(q_0)$ is given by a sum of two terms, where the former contains perturbative contributions up to two loops. For comparison, we also plot the result of perturbative calculations up to and including 7 loops. It is seen that, for a given

JHEP10(2025)197

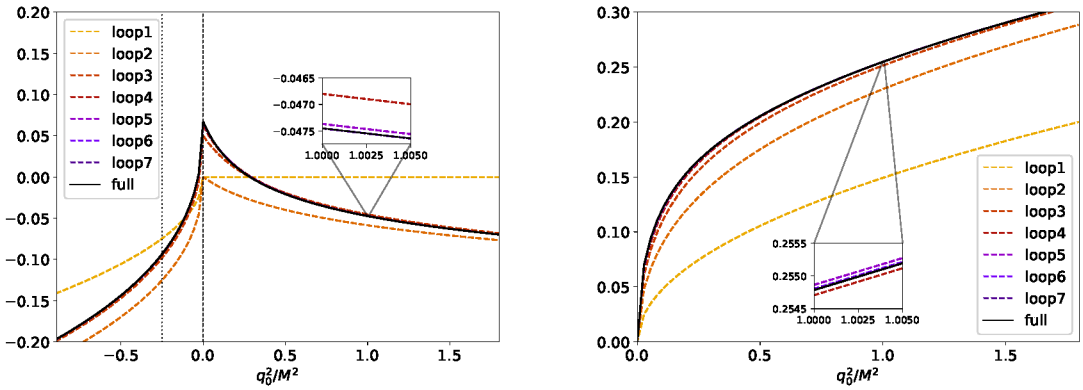

Figure 9. The real and imaginary parts of the function $M_\ell(q_0)$ for $\ell = 0$. The imaginary part is zero below threshold. The full solution corresponds to the sum of the $M_\ell^{\text{div}}(q_0)$ (up to two loops) and $M_\ell^{\text{fin}}(q_0)$, see eq. (4.1). For comparison, the perturbative result up to 7 loops is shown. The vertical lines in the left panel correspond to the elastic threshold and the beginning of the left-hand cut.

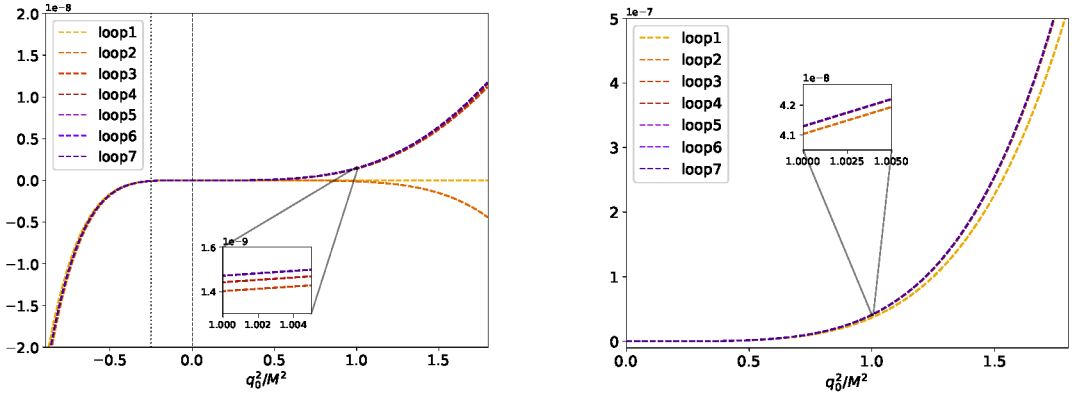

Figure 10. The real and imaginary parts of the function $M_\ell(q_0)$ for $\ell = 4$. The imaginary part is zero below threshold. The perturbative expansion converges very rapidly, so that the contribution of $M_\ell^{\text{fin}}(q_0)$ is invisible by the bare eye and is not shown (see also the zoomed-in windows). The vertical lines in the left panel correspond to the elastic threshold and the beginning of the left-hand cut.

value of the coupling g, the perturbative series converges rapidly, so the result in 4 loops and higher becomes visually indistinguishable from the full solution.

In figure 10 the result of the calculation in case $\ell = 4$ is shown. Now, $M_\ell^{\text{div}}(q_0)$ contains 10 terms, and $M_\ell^{\text{fin}}(q_0)$ is so small that it cannot be distinguished with a bare eye. As one sees from the figure, the convergence is again very good and, after calculating a few loops, the full solution does not change anymore. Note that oscillations in the real part are an artifact of the subtraction and do not have an effect on the convergence.

Last but not least, note that only repulsive interactions are considered in the present paper. In case of attractive interactions, bound states can emerge in the spectrum and the Born series is no longer convergent. In our approach, these bound state poles show up in $M_\ell^{\text{fin}}(q_0)$.

JHEP10(2025)197

4.3 Coulomb interactions

In the limit $M \to 0$, our long-range force reduces to the Coulomb force, for which the analytic solution is known [30, 31]. In this case, we have to identify the dimensionful constant g with $g = 2\mu_r\alpha$, where μ_r is the reduced mass and α denotes the fine structure constant. The quantity $M_\ell(q_0)$ becomes the function of the dimensionless variable $\eta = \alpha\mu_r/q_0$. Restricting ourselves, for simplicity, to the case $\ell = 0$, we get

$$M_0(q_0) = 2\alpha\mu_r\left\{\eta^2\sum_{n=1}^{\infty}\frac{1}{n(n^2+\eta^2)} - \log\eta + \Gamma'(1)\right\}. \tag{4.28}$$

We have checked that, in the limit $M \to 0$, the expression in the curly brackets in eq. (4.11) indeed yields the term $-\log\eta$ up to an inessential constant contribution. Fixing of this contribution amounts to setting the renormalization prescription. Higher order terms in the expansion in η are obtained from the multi-loop integrals. The loops with odd N are purely imaginary and do not contribute. We have (numerically) checked that the first few coefficients of the expansion of $M_\ell(q_0)$ indeed reproduce those obtained from eq. (4.28) with a very good precision. Thus, our expression for $M_\ell(q_0)$ indeed reduces to the known one from refs. [30, 31] in the massless limit.

4.4 Modified effective range expansion function

As mentioned above, the modified quantization condition allows one to extract the modified effective range function $K_\ell^M(q_0^2)$ both above and below threshold and, in particular, in the left-land cut region where the standard Lüscher approach fails. Here we wish to construct $K_\ell^M(q_0^2)$ in the whole energy range and ensure that it is smooth and real everywhere, in contrast to the standard K-matrix. We carry out calculations in the model described by the potential (3.10) and restrict ourselves, for simplicity, to the case $\ell = 0$.

It should be pointed out that the analytic continuation of the solution of the Lippmann-Schwinger equation below threshold is by no means a trivial affair. As discussed, e.g., in ref. [32], when $q_0^2 < -M^2$, the path of momentum integration in the Lippmann-Schwinger integration, which originally runs from 0 to infinity, should be deformed in order to avoid the singularities of the potential. The left-hand cut starts higher, at $q_0^2 = -M^2/4$. Since the analysis in the left-hand cut region is our primary interest in this paper, we restrict the energy interval by $q_0^2 > -M^2$. Albeit, with some additional effort, the analysis can be extended to the larger region $q_0^2 > -M_S^2/4$.

Another subtle issue is the definition of the effective range expansion below threshold. The definition (2.4) applies above threshold. In the interval $-M^2 < q_0^2 < 0$ we use the following definition:

$$K_\ell^M(q_0^2) = M_\ell(q_0) + \frac{4\pi q_0^{2\ell}}{|f_\ell(q_0)|^2}\,\frac{1}{T_\ell(q_0) - T_\ell^L(q_0)}\,, \tag{4.29}$$

where $T_\ell(q_0), T_\ell^L(q_0)$ denote the full and the long range fully on-shell scattering amplitudes (these amplitudes become complex in the left-hand cut region, however the difference $T_\ell(q_0) - T_\ell^L(q_0)$ stays real). The Jost function is also real in the considered subthreshold interval

JHEP10(2025)197

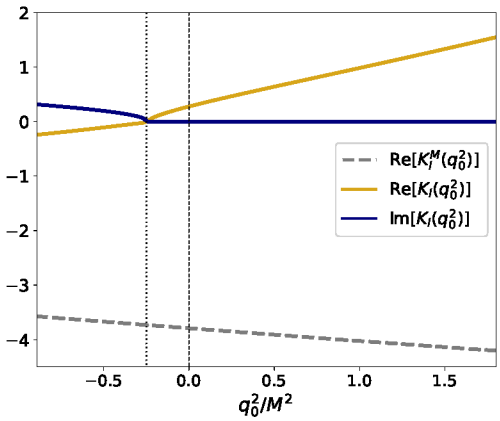

Figure 11. Real and imaginary parts (in arbitrary units) of the standard effective range function $K_\ell(q_0^2)$ (solid lines) vs. the real part of the modified effective range function $K_\ell^M(q_0^2)$ (dashed line) in the S-wave ($\ell = 0$). The imaginary part of $K_\ell^M(q_0^2)$ is zero everywhere in the interval considered. The position of the left-hand threshold is shown by a vertical dotted line.

and is given by

$$f_\ell(q_0)^{-1} = 1 + \frac{1}{q_0^\ell} \int_0^\infty \frac{p^2 dp}{2\pi^2} \frac{p^\ell}{p^2 - q_0^2} T_\ell^L(p, q_0; q_0^2)\,, \qquad T_\ell^L(q_0) = T_\ell^L(p, q_0; q_0^2)\,. \quad (4.30)$$

In figure 11 we show the modified effective range function $K_\ell^M(q_0^2)$ vs. the standard one $K_\ell(q_0^2)$. The difference is clearly visible. While the standard function displays a singular structure at the left-land threshold and becomes complex below it, the modified effective range function is almost linear in the whole interval considered. Moreover, it does not demonstrate any sign of a singular behavior even very close to $q_0^2 = -M^2$, in agreement with the claim that the convergence radius of the modified effective range expansion is set by the short-range scale M_S.

5 Conclusions

i) In the present paper we discussed the numerical implementation of the modified Lüscher equation, proposed in ref. [1]. We chose to demonstrate the essential features of the implementation, using a simple toy model: two spinless non-relativistic particles interacting through a sum of two Yukawa potentials, having different ranges. Furthermore, the center-of-mass frame was chosen from the beginning, and we restricted ourselves to the case of the A_1^+ irrep of the octahedral group only. All these are purely technical restrictions and can be easily removed in the analysis of real lattice data.

ii) In addition to the above, we assumed that the long-range force is perturbative and does not create bound states/low-lying resonances alone. In contrast to the other assumptions, this one is more restrictive and might require additional scrutiny. For the time being, we however stick to this assumption, because it is justified for the real physical systems which are studied on the lattice at present.

JHEP10(2025)197

iii) We went step by step and presented a simple but rather accurate and fast algorithm for the calculation of the modified Lüscher zeta-function shown in figure 1. This quantity is ultraviolet-divergent as its renormalization is a non-trivial issue, especially in higher partial waves. From the point of numerical algorithms, a cutoff is a preferred choice. However, cutoff regularization leads to the very large subtraction terms in higher partial waves that affects the accuracy of calculations. From this point of view, dimensional regularization is preferred because in this case the subtraction terms are of natural size in all partial waves. We derive explicit expressions for the renormalized n-loop exchange diagrams in dimensional regularization, using a subtraction scheme that does not produce unnaturally large polynomial contributions.

iv) The solutions of the quantization condition (both modified and standard ones) are compared with the exact finite-volume spectrum of the Hamiltonian, calculated in the plane-wave basis. The results confirm all our expectations. First of all, exponential corrections are very small for all levels except the ground state, where they are increased owing to the proximity of the left-hand cut. Furthermore, the convergence of the partial-wave expansion is very good in the modified case and poor in the standard case. Indeed, the standard case implies the partial-wave expansion of the whole potential, whereas in the modified case only the short-range potential is expanded in partial waves, the long-range part is treated in the plane-wave basis as a whole.

v) If the modified Lüscher zeta-function for a known long-range potential is calculated and tabulated in advance, the analysis of lattice data proceeds exactly in the same manner as in the case of the standard Lüscher equation. The truncation in partial waves, which involves short-range potential only, is justified. This potentially renders the proposed approach very convenient for the analysis of lattice data.

vi) The long-range potential considered in the present paper corresponds to the exchange of a particle with the nonzero mass M. The asymptotic wave function in such a potential has still a conventional form, and standard boundary conditions imposed on the Jost functions lead to the unitary S-matrix. Modifications needed in case of the inclusion of the Coulomb force form a subject of a separate investigation.

Acknowledgments

The authors especially acknowledge the contribution from Fabian Müller, who intensively collaborated with us at the early stage of the project. We thank E. Epelbaum, A. Gasparyan, B. Metsch and Yan Li for useful discussions. The work of R.B, F.M. and A.R. was funded in part by the Deutsche Forschungsgemeinschaft (DFG, German Research Foundation) under Project-ID 196253076 — TRR 110 and by the Ministry of Culture and Science of North Rhine-Westphalia through the NRW-FAIR project. A.R., in addition, thanks the Chinese Academy of Sciences (CAS) President's International Fellowship Initiative (PIFI) (grant no. 2024VMB0001) for the partial financial support. The work of J.-Y.P. and J.-J.W. was supported by the National Natural Science Foundation of China (NSFC) under Grants No. 12135011, 12175239, 12221005, and by the National Key R&D Program of China under

JHEP10(2025)197

Contract No. 2020YFA0406400, and by the Chinese Academy of Sciences under Grant No. YSBR-101. H.-W.H. was supported by Deutsche Forschungsgemeinschaft (DFG, German Research Foundation) under Project-ID 279384907 — SFB 1245 and by the German Federal Ministry of Education and Research (BMBF) (Grant No. 05P24RDB). B.-L. H. was supported by the DFG through the Research Unit "Photon–photon interactions in the Standard Model and beyond" (Projektnummer 458854507 — FOR 5327).

A Partial-wave contributions to the energy shift of a given state

In this appendix, we give a qualitative explanation for the uneven convergence of the partial-wave expansion, which is observed in figure 6. We shall namely argue that the pattern of the convergence in different excited states can be understood solely on the basis of a symmetry argument.

In the beginning, let us note that the energy shifts from the unperturbed states are generally small, so first-order perturbation theory captures the bulk of the effect. These unperturbed states represent the finite-volume momentum eigenstates $|\boldsymbol{n}\rangle$ that satisfy the completeness condition

$$\sum_{\boldsymbol{n}\in\mathbb{Z}^3} |\boldsymbol{n}\rangle\langle\boldsymbol{n}| = \mathbb{1}. \tag{A.1}$$

Let us now introduce the *shells* — sets of vectors generated from a given vector $|\boldsymbol{n}\rangle$ by the action of all elements of the octahedral group O_h. We label these shells by index r. It is clear that the matrix representations of O_h can be realized in the linear space spanned by all vectors belonging to a given shell. These representations are in general reducible, and can be decomposed into the different irreps. There are seven fundamental types of shells (see, e.g. [2, 33, 34]), classified according to how many components of the three-momentum share the same magnitude. The decomposition of the representations of the group O_h for these shells are given by

$$\begin{aligned}
(0,0,0): &\quad A_1^+\,,\\
(0,0,c): &\quad A_1^+ \oplus E^+ \oplus T_1^-\,,\\
(0,b,b): &\quad A_1^+ \oplus E^+ \oplus T_1^- \oplus T_2^+ \oplus T_2^-\,,\\
(0,b,c): &\quad A_1^+ \oplus A_2^+ \oplus 2E^+ \oplus T_1^+ \oplus 2T_1^- \oplus T_2^+ \oplus 2T_2^-\,,\\
(a,a,a): &\quad A_1^+ \oplus A_2^- \oplus T_1^- \oplus T_2^+\,,\\
(a,a,c): &\quad A_1^+ \oplus A_2^- \oplus E^+ \oplus E^- \oplus T_1^+ \oplus 2T_1^- \oplus 2T_2^+ \oplus T_2^-\,,\\
(a,b,c): &\quad A_1^+ \oplus A_1^- \oplus A_2^+ \oplus A_2^- \oplus 2E^+ \oplus 2E^- \oplus 3T_1^+ \oplus 3T_1^- \oplus 3T_2^+ \oplus 3T_2^-\,.
\end{aligned} \tag{A.2}$$

We denote the basis vectors for each irrep by $|\Gamma t,\alpha;r\rangle$. Here Γ labels the irrep of O_h, α distinguishes the basis vectors within that irrep, r labels shells and t enumerates the multiplicity of the irrep Γ [34].

Let us now evaluate the finite-volume energy shift of an unperturbed state $|\boldsymbol{n}\rangle$. When the interaction is switched on, the level splitting occurs, and the states belonging to the different irreps are shifted differently. For a given interaction potential V, the leading-order

JHEP10(2025)197

perturbative energy shift of a state transforming in the irrep Γ is obtained by diagonalization of the following matrix in the space of indices t, t':

$$V_{tt'}^{(\Gamma)}(r) = \langle \Gamma t, \alpha; r | V | \Gamma t', \alpha; r \rangle. \tag{A.3}$$

Here α is arbitrary due to the Wigner-Eckart theorem.

Furthermore, the interaction potential can be expanded in partial waves:

$$\langle \boldsymbol{n}_1 | V | \boldsymbol{n}_2 \rangle = 4\pi \sum_{\ell m} Y_{\ell m}(\hat{\boldsymbol{n}}_1) V_\ell(p_1, p_2) Y_{\ell m}^*(\hat{\boldsymbol{n}}_2), \tag{A.4}$$

where $p_i = \dfrac{2\pi}{L}|\boldsymbol{n}_i|$. Therefore, the matrix element in eq. (A.3) is given by

$$\begin{aligned} V_{tt'}^{(\Gamma)}(r) &= \sum_{\boldsymbol{n}_1, \boldsymbol{n}_2 \in \text{shell-}r} \langle \Gamma t, \alpha; r | \boldsymbol{n}_1 \rangle \langle \boldsymbol{n}_1 | V | \boldsymbol{n}_2 \rangle \langle \boldsymbol{n}_2 | \Gamma t', \alpha; r \rangle \\ &= 4\pi \sum_{\ell m} V_\ell(p_1, p_2) \sum_{\boldsymbol{n}_1, \boldsymbol{n}_2 \in \text{shell-}r} \langle \Gamma t, \alpha; r | \boldsymbol{n}_1 \rangle Y_{\ell m}(\hat{\boldsymbol{n}}_1) Y_{\ell m}^*(\hat{\boldsymbol{n}}_2) \langle \boldsymbol{n}_2 | \Gamma t', \alpha; r \rangle \,. \end{aligned} \tag{A.5}$$

Note that since $\boldsymbol{n}_1$ and $\boldsymbol{n}_2$ both belong to the shell-r, $p_1 = p_2$ is the magnitude of the three-momentum in the shell-r.

Next, we introduce the finite-volume partial-wave states $|\ell, m; r\rangle$, defined through projecting the plane-wave basis onto the spherical harmonics [34]

$$|\ell, m; r\rangle = \sum_{\boldsymbol{n} \in \text{shell-}r} \sqrt{4\pi}\, Y_{\ell m}(\hat{\boldsymbol{n}})\, |\boldsymbol{n}\rangle \,, \tag{A.6}$$

and define

$$|\Gamma t \ell, \alpha; r\rangle = \sum_m c_{\ell m}^{\Gamma \alpha t} |\ell, m; r\rangle \,, \tag{A.7}$$

where $c_{\ell m}^{\Gamma \alpha t}$ denotes the pertinent Clebsh-Gordan coefficient, see, e.g., eq. (2.9). Since the transformation between $|\ell, m; r\rangle$ and $|\Gamma t \ell, \alpha; r\rangle$ is unitary, we have

$$\sum_m |\ell, m; r\rangle \langle \ell, m; r| = \sum_{\Gamma t \alpha} |\Gamma t \ell, \alpha; r\rangle \langle \Gamma t \ell, \alpha; r| \,. \tag{A.8}$$

This means that

$$\begin{aligned} V_{tt'}^{(\Gamma)}(r) &= 4\pi \sum_{\ell m} V_\ell(p, p) \sum_{\boldsymbol{n}_1, \boldsymbol{n}_2 \in \text{shell-}r} \langle \Gamma t, \alpha; r | \boldsymbol{n}_1 \rangle Y_{\ell m}(\hat{\boldsymbol{n}}_1) Y_{\ell m}^*(\hat{\boldsymbol{n}}_2) \langle \boldsymbol{n}_2 | \Gamma t', \alpha; r \rangle \\ &= \sum_{\ell m} V_\ell(p, p) \langle \Gamma t, \alpha; r | \ell, m; r \rangle \langle \ell, m; r | \Gamma t', \alpha; r \rangle \\ &= \sum_{\ell} V_\ell(p, p) \sum_{\Gamma' t'' \beta} \langle \Gamma t, \alpha; r | \Gamma' t'' \ell, \beta; r \rangle \langle \Gamma' t'' \ell, \beta; r | \Gamma t', \alpha; r \rangle \\ &= \sum_{\ell} V_\ell(p, p) \sum_{t''} \langle \Gamma t, \alpha; r | \Gamma t'' \ell, \alpha; r \rangle \langle \Gamma t'' \ell, \alpha; r | \Gamma t', \alpha; r \rangle. \end{aligned} \tag{A.9}$$

Now let us define

$$G_{\ell, tt'}^{(\Gamma)}(r) = \sum_{t''} \langle \Gamma t, \alpha; r | \Gamma t'' \ell, \alpha; r \rangle \langle \Gamma t'' \ell, \alpha; r | \Gamma t', \alpha; r \rangle. \tag{A.10}$$

JHEP10(2025)197

The quantity G was calculated in ref. [34]. In order to understand the result presented in figure 6, we restrict ourselves to the irrep $\Gamma = A_1^+$ and truncate the partial-wave expansion, keeping only $\ell = 0, 4$. In this case, the multiplicities t, t', t'' and the label of the basis vector, α, all take a single value. For simplicity, we shall ignore these indices in the following. The leading-order energy shift then reduces to

$$\Delta E^{(A_1^+)}(r) = V^{(A_1^+)}(r) = G_0^{(A_1^+)}(r) V_0(p,p) + G_4^{(A_1^+)}(r) V_4(p,p) + \cdots . \tag{A.11}$$

The quantity G is given by

$$G_\ell^{(A_1^+)}(r) = |\langle A_1^+; r | A_1^+ \ell; r \rangle|^2 . \tag{A.12}$$

This quantity can be evaluated directly, resulting in

$$\begin{aligned}
(000): &\quad G_0^{(A_1^+)} = 1\,, &\quad G_4^{(A_1^+)} &= 0\,,\\
(001): &\quad G_0^{(A_1^+)} = 6\,, &\quad G_4^{(A_1^+)} &= 31.5\,,\\
(011): &\quad G_0^{(A_1^+)} = 12\,, &\quad G_4^{(A_1^+)} &= 3.94\,,\\
(012): &\quad G_0^{(A_1^+)} = 24\,, &\quad G_4^{(A_1^+)} &= 5.04\,,\\
(111): &\quad G_0^{(A_1^+)} = 8\,, &\quad G_4^{(A_1^+)} &= 18.67\,,\\
(112): &\quad G_0^{(A_1^+)} = 24\,, &\quad G_4^{(A_1^+)} &= 7.88\,,\\
(123): &\quad G_0^{(A_1^+)} = 48\,, &\quad G_4^{(A_1^+)} &= 15.75\,.
\end{aligned} \tag{A.13}$$

The seven cases above correspond to the seven types of the momentum shells. Relatively large $G_4^{(A_1^+)}$ factors associated with the shells (001) and (111) are responsible for sizable G-wave contributions to the first and third excited states. And, *vice versa,* much smaller $G_4^{(A_1^+)}$ factors for (011), (012) and (112) shells explain, why the G-wave corrections are negligible in the second, fifth, and sixth excited states, see figure 6.

Data Availability Statement. This article has no associated data or the data will not be deposited.

Code Availability Statement. This article has no associated code or the code will not be deposited.

References

[1] R. Bubna et al., *Lüscher equation with long-range forces*, *JHEP* **05** (2024) 168 [arXiv:2402.12985] [INSPIRE].

[2] L. Meng and E. Epelbaum, *Two-particle scattering from finite-volume quantization conditions using the plane wave basis*, *JHEP* **10** (2021) 051 [arXiv:2108.02709] [INSPIRE].

JHEP10(2025)197

[3] L. Meng et al., *Solving the left-hand cut problem in lattice QCD: Tcc(3875)+ from finite volume energy levels*, *Phys. Rev. D* **109** (2024) L071506 [arXiv:2312.01930] [INSPIRE].

[4] A.B. Raposo and M.T. Hansen, *Finite-volume scattering on the left-hand cut*, *JHEP* **08** (2024) 075 [arXiv:2311.18793] [INSPIRE].

[5] A.B. Raposo, R.A. Briceño, M.T. Hansen and A.W. Jackura, *Extracting scattering amplitudes for arbitrary two-particle systems with one-particle left-hand cuts via lattice QCD*, *JHEP* **06** (2025) 186 [arXiv:2502.19375] [INSPIRE].

[6] M.T. Hansen, F. Romero-López and S.R. Sharpe, *Incorporating $DD\pi$ effects and left-hand cuts in lattice QCD studies of the $T_{cc}(3875)^+$*, *JHEP* **06** (2024) 051 [arXiv:2401.06609] [INSPIRE].

[7] S.M. Dawid, F. Romero-López and S.R. Sharpe, *Finite- and infinite-volume study of $DD\pi$ scattering*, *JHEP* **01** (2025) 060 [arXiv:2409.17059] [INSPIRE].

[8] S.M. Dawid, A.W. Jackura and A.P. Szczepaniak, *Finite-volume quantization condition from the N/D representation*, *Phys. Lett. B* **864** (2025) 139442 [arXiv:2411.15730] [INSPIRE].

[9] M. Abolnikov et al., *Internal structure of the Tcc(3875)+ from its light-quark mass dependence*, *Phys. Lett. B* **860** (2025) 139188 [arXiv:2407.04649] [INSPIRE].

[10] M.-L. Du, F.-K. Guo and B. Wu, *Effective range expansion with the left-hand cut and its application to the $T_{cc}(3875)$*, in the proceedings of the *11th International Workshop on Chiral Dynamics — PoS(CD2024)*, Ruhr University Bochum, Germany, 26–30 August 2024 [DOI:10.22323/1.479.0062].

[11] S.M. Dawid, F. Romero-López and S.R. Sharpe, *Comparison of integral equations used to study T_{cc}^+ for a stable D^**, *JHEP* **09** (2025) 058 [arXiv:2505.05466] [INSPIRE].

[12] K. Yu, G.-J. Wang, J.-J. Wu and Z. Yang, *Finite volume Hamiltonian method for two-particle systems containing long-range potential on the lattice*, *JHEP* **04** (2025) 108 [arXiv:2502.05789] [INSPIRE].

[13] Hadron Spectrum collaboration, *Near-threshold states in coupled DD^*-D^*D^* scattering from lattice QCD*, *Phys. Rev. D* **111** (2025) 034511 [arXiv:2405.15741] [INSPIRE].

[14] S. Collins, A. Nefediev, M. Padmanath and S. Prelovsek, *Toward the quark mass dependence of Tcc+ from lattice QCD*, *Phys. Rev. D* **109** (2024) 094509 [arXiv:2402.14715] [INSPIRE].

[15] S. Prelovsek et al., *Doubly heavy tetraquarks from lattice QCD: Incorporating diquark-antidiquark operators and the left-hand cut*, *Phys. Rev. D* **112** (2025) 014507 [arXiv:2504.03473] [INSPIRE].

[16] L. Meng et al., *Doubly charm tetraquark channel with isospin 1 from lattice QCD*, *Phys. Rev. D* **111** (2025) 034509 [arXiv:2411.06266] [INSPIRE].

[17] J.R. Green, A.D. Hanlon, P.M. Junnarkar and H. Wittig, *Weakly bound H dibaryon from SU(3)-flavor-symmetric QCD*, *Phys. Rev. Lett.* **127** (2021) 242003 [arXiv:2103.01054] [INSPIRE].

[18] S. Amarasinghe et al., *Variational study of two-nucleon systems with lattice QCD*, *Phys. Rev. D* **107** (2023) 094508 [*Erratum ibid.* **110** (2024) 119904] [arXiv:2108.10835] [INSPIRE].

[19] J. Green, *Status of two-baryon scattering in lattice QCD*, in the proceedings of the *11th International Workshop on Chiral Dynamics — PoS(CD2024)*, Ruhr University Bochum, Germany, 26–30 August 2024 [DOI:10.22323/1.479.0019].

[20] S. Aoki and T. Doi, *Lattice QCD and baryon-baryon interactions: HAL QCD method*, *Front. in Phys.* **8** (2020) 307 [arXiv:2003.10730] [INSPIRE].

JHEP10(2025)197

[21] Y. Lyu et al., *Doubly Charmed Tetraquark Tcc+ from Lattice QCD near Physical Point*, *Phys. Rev. Lett.* **131** (2023) 161901 [arXiv:2302.04505] [INSPIRE].

[22] S. Aoki, T. Doi and Y. Lyu, *Left-hand cut and the HAL QCD method*, *PoS* **LATTICE2024** (2025) 089 [arXiv:2501.16804] [INSPIRE].

[23] M. Luscher, *Two particle states on a torus and their relation to the scattering matrix*, *Nucl. Phys. B* **354** (1991) 531 [INSPIRE].

[24] H. van Haeringen and L.P. Kok, *Modified effective range function*, *Phys. Rev. A* **26** (1982) 1218 [INSPIRE].

[25] V. Bernard, M. Lage, U.-G. Meissner and A. Rusetsky, *Resonance properties from the finite-volume energy spectrum*, *JHEP* **08** (2008) 024 [arXiv:0806.4495] [INSPIRE].

[26] M. Gockeler et al., *Scattering phases for meson and baryon resonances on general moving-frame lattices*, *Phys. Rev. D* **86** (2012) 094513 [arXiv:1206.4141] [INSPIRE].

[27] D. Minossi, E. Epelbaum, M. Pavón Valderrama and A. Nogga, *Modified effective range expansion for nucleon-nucleon scattering*, *EPJ Web Conf.* **3** (2010) 05018.

[28] G.P. Lepage, *A New Algorithm for Adaptive Multidimensional Integration*, *J. Comput. Phys.* **27** (1978) 192 [INSPIRE].

[29] G.P. Lepage, *Adaptive multidimensional integration: VEGAS enhanced*, *J. Comput. Phys.* **439** (2021) 110386 [arXiv:2009.05112] [INSPIRE].

[30] H.A. Bethe, *Theory of the Effective Range in Nuclear Scattering*, *Phys. Rev.* **76** (1949) 38 [INSPIRE].

[31] G.F. Chew and M.L. Goldberger, *On the Analysis of Nucleon-Nucleon Scattering Experiments*, *Phys. Rev.* **75** (1949) 1637 [INSPIRE].

[32] J.A. Oller and D.R. Entem, *The exact discontinuity of a partial wave along the left-hand cut and the exact N/D method in non-relativistic scattering*, *Annals Phys.* **411** (2019) 167965 [arXiv:1810.12242] [INSPIRE].

[33] M. Döring et al., *Three-body spectrum in a finite volume: the role of cubic symmetry*, *Phys. Rev. D* **97** (2018) 114508 [arXiv:1802.03362] [INSPIRE].

[34] Y. Li et al., *Partial Wave Mixing in Hamiltonian Effective Field Theory*, *Phys. Rev. D* **101** (2020) 114501 [arXiv:1910.04973] [INSPIRE].

JHEP10(2025)197